Molecular Therapy
Methods & Clinical Development
Original Article

Circulating neurofilament light chain as a promising biomarker of AAV-induced dorsal root ganglia toxicity in nonclinical toxicology species

Kelly A. Fader,[1] Ingrid D. Pardo,[2] Ramesh C. Kovi,[3] Christopher J. Somps,[1] Helen Hong Wang,[3] Vishal S. Vaidya,[3] Shashi K. Ramaiah,[3] and Madhu P. Sirivelu[3]

[1]Pfizer Worldwide Research, Development and Medical, Drug Safety Research and Development, Groton, CT 06340, USA; [2]Biogen, Cambridge, MA 02142, USA; [3]Pfizer Worldwide Research, Development and Medical, Drug Safety Research and Development, Pfizer Inc., 300 Technology Square, Cambridge, MA 02139, USA

Adeno-associated virus (AAV)-induced dorsal root ganglia (DRG) toxicity has been observed in several nonclinical species, where lesions are characterized by neuronal degeneration/necrosis, nerve fiber degeneration, and mononuclear cell infiltration. As AAV vectors become an increasingly common platform for novel therapeutics, non-invasive biomarkers are needed to better characterize and manage the risk of DRG neurotoxicity in both nonclinical and clinical studies. Based on biological relevance, reagent availability, antibody cross-reactivity, DRG protein expression, and assay performance, neurofilament light chain (NF-L) emerged as a promising biomarker candidate. Dose- and time-dependent changes in NF-L were evaluated in male Wistar Han rats and cynomolgus monkeys following intravenous or intrathecal AAV injection, respectively. NF-L profiles were then compared against microscopic DRG lesions on day 29 post-dosing. In animals exhibiting DRG toxicity, plasma/serum NF-L was strongly associated with the severity of neuronal degeneration/necrosis and nerve fiber degeneration, with elevations beginning as early as day 8 in rats ($\geq 5 \times 10^{13}$ vg/kg) and day 14 in monkeys ($\geq 3.3 \times 10^{13}$ vg/dose). Consistent with the unique positioning of DRGs outside the blood-brain barrier, NF-L in cerebrospinal fluid was only weakly associated with DRG findings. In summary, circulating NF-L is a promising biomarker of AAV-induced DRG toxicity in nonclinical species.

INTRODUCTION

Adeno-associated virus (AAV)-based vectors have emerged as one of the most frequently used approaches for gene therapy, whereby nucleic acids are introduced into host cells to replace, suppress, or repair a gene. AAV is a naturally occurring, non-enveloped virus that contains a linear single-stranded DNA genome of ~4.7 kilobases (kb).[1] Flanked between inverted terminal repeats (ITRs), the coding sequences of the genome can be replaced by a gene of interest and strategic promoter to yield a recombinant AAV (rAAV) vector. rAAVs are ideal for gene therapy given their (1) favorable safety profile, (2) deficient replication, (3) efficient transduction, which results in stable expression in non-dividing cells, and (4) a relatively low frequency of integration into the host DNA compared with other vectors.[2,3] In addition, the various AAV serotypes exhibit preferred tropism for certain tissues, which can be combined with tissue-specific promoters or enhancers to design a selective gene therapy strategy.[4]

Despite these advantages, challenges have arisen during the development of rAAV-based gene therapy, including a limited packaging capacity (<4.7 kb), dilution of vector genomes in actively dividing cells, and rapidly evolving regulatory requirements. In addition, four major categories of potential AAV-induced toxicity have been identified: (1) immunogenicity, (2) hepatotoxicity, (3) insertional mutagenesis, and (4) dorsal root ganglia (DRG) toxicity.[3,5] AAV-mediated immunogenicity typically involves T cell and humoral responses to the vector capsid or transgene product, which may lead to death of the transduced cells and loss of therapeutic efficacy.[6–8] In clinical practice, anti-capsid inflammatory responses have been shown to be suppressed or resolved by co-administering AAV vectors with corticosteroids,[9] while rapamycin is reported to prevent humoral and cell-mediated responses in preclinical models.[10,11] Hepatic necrosis and coagulopathy have been observed in non-human primates (NHPs) treated with high doses of AAV,[12,13] while acute liver failure has been reported in two infants following treatment with an AAV vector containing the survival motor neuron 1 (*SMN1*) gene (onasemnogene abeparvovec).[14] Moreover, neonatal mice are reported to develop hepatocellular carcinoma following AAV integration at the RNA imprinted and accumulated in nucleus (*Rian*) locus.[15,16] However, insertional mutagenesis has not been observed in adult mice or other nonclinical species, suggesting a species- and age-dependent mechanism.

Following AAV administration, NHPs and rodents exhibit a high incidence of microscopic DRG lesions, although clinical sensory

Received 3 January 2022; accepted 27 March 2022;
https://doi.org/10.1016/j.omtm.2022.03.017.

Correspondence: Madhu P. Sirivelu, Pfizer Worldwide Research, Development and Medical, Drug Safety Research and Development, Pfizer Inc., 300 Technology Square, Cambridge, MA, 02139.
E-mail: madhu.sirivelu@pfizer.com

Table 1. Group incidence and severity of dorsal root ganglia microscopic findings in male Wistar Han rats

Dose (vg/kg)	0	2×10^{13}	5×10^{13}	1×10^{14}
n per group	6	6	6	6
Neuron Degeneration/Necrosis	0	0	5	6
Minimal (Grade 1)	0	0	3	3
Mild (Grade 2)	0	0	2	3
Nerve Fiber Degeneration	1	1	5	6
Minimal (Grade 1)	1	1	4	0
Mild (Grade 2)	0	0	0	3
Moderate (Grade 3)	0	0	1	3
Mononuclear Cell Infiltration	0	0	3	6
Minimal (Grade 1)	0	0	1	6
Mild (Grade 2)	0	0	2	0
Satellite Glial Cell Hypertrophy/Hyperplasia	0	0	2	6
Minimal (Grade 1)	0	0	0	3
Mild (Grade 2)	0	0	2	3

deficits are rarely observed.[5,12,13,17–21] These dose-dependent lesions are characterized by neuronal degeneration and/or necrosis, nerve fiber degeneration, and mononuclear cell infiltration. In one study, AAV-treated piglets exhibited severe DRG lesions accompanied by neurological deficits such as ataxia and impairments in conscious proprioception.[13] A meta-analysis of 33 AAV studies involving 256 NHPs (rhesus and cynomolgus) revealed histopathological DRG findings across (1) five different capsids, (2) five different promoters, (3) 20 different transgenes, (4) three routes of administration (intravenous, intra-cisterna magna, intrathecal), and (5) two methods of vector purification (column-purified, iodixanol-purified). Dose and age at injection were found to significantly affect the severity of neuronal lesions, while sex had no impact.[22] Taken together, these studies suggest DRG toxicity in nonclinical species is driven by the AAV modality itself rather than any specific therapeutic target. Comparable to these DRG findings, neuronal degeneration/necrosis and nerve fiber degeneration have also been observed in trigeminal and autonomic ganglia from AAV-treated rats and cynomolgus monkeys, indicating various ganglia throughout the body are affected.[12] In humans, sensory deficits (meningoradiculitis) were observed in one of two familial amyotrophic lateral sclerosis (ALS) patients following an intrathecal infusion of AAV containing anti-superoxide dismutase 1 (*SOD1*) microRNA.[23] Beyond this single report, the human relevance of AAV-induced ganglia toxicity is currently unknown.

The risk of AAV-induced DRG toxicity could be mitigated by repressing or controlling transgene expression in DRG sensory neurons. Specific mitigation strategies proposed to date include (1) use of AAV serotypes (e.g., AAV3) with lower transduction potential for DRG neurons,[24] (2) use of non-neuronal tissue-specific promoters which restrict transgene expression to the target tissue,[25] and (3) inclusion of regulatory elements in the transgene cassette.[26] For example, endogenous expression of miR-183 is highly enriched within DRG sensory neurons.[27] Therefore, incorporating an miR-183 recognition site within the vector genome has been shown to reduce both transgene expression and toxicity within DRG neurons without affecting transduction in other nervous system tissues.[17]

At present, there are no reports of circulating biomarkers available for assessing AAV-induced DRG toxicity in either preclinical models or humans. As rAAV vectors become an increasingly common platform for novel therapeutics, non-invasive biomarkers are needed to better characterize and evaluate the risk of DRG neurotoxicity in both nonclinical and clinical studies. The objectives of this research were to (1) identify non-invasive safety biomarker(s) for assessing AAV-induced DRG lesions in nonclinical species, and (2) develop an in-house assay for quantifying this biomarker. We demonstrate that NF-L is a promising biomarker of AAV-induced DRG toxicity in rats and cynomolgus monkeys, where plasma/serum increases were strongly associated with the severity of neuron degeneration/necrosis and nerve fiber degeneration.

RESULTS

Histologic DRG findings in AAV-treated rats and cynomolgus monkeys

Histopathological evaluation of H&E-stained sections of nerves attached to DRGs and neurons within DRGs revealed dose-dependent AAV-induced toxicity in male Wistar Han rats (Table 1; Figure 1) and cynomolgus monkeys (Table 2; Figure 2). This included minimal to moderate neuronal degeneration/necrosis, nerve fiber degeneration, and mononuclear cell infiltration in DRGs (cervical, thoracic, and lumbar regions). Nerve fiber degeneration occurred in dorsal and spinal nerve roots (sensory axons). In addition, minimal to mild satellite glial cell hypertrophy/hyperplasia was observed exclusively in rats. In the rat study, one control and one low-dose (2×10^{13} vg/kg) animal exhibited minimal nerve fiber degeneration (dorsal and/or spinal nerve roots), while all other findings were observed at $\geq 5 \times 10^{13}$ vg/kg. Given that minimal nerve fiber degeneration is not uncommon in rats and other laboratory animals,[28] this lesion was considered a background finding. In cynomolgus monkeys, neuronal and/or nerve fiber degeneration were observed at 3.3×10^{13} vg/dose [3x] and 8.7×10^{13} vg/dose [1x]. Despite receiving a lower total dose, one animal in the 8.7×10^{13} vg group exhibited more severe DRG lesions (moderate neuron/nerve fiber degeneration, mononuclear cell infiltration) than either animal receiving three injections of 3.3×10^{13} vg/dose (total = 1.0×10^{14} vg/animal). In both species, dose-dependent, minimal to mild multifocal nerve fiber degeneration was also observed in the dorsal funiculi (ascending sensory axons with cell bodies in the DRGs) of the spinal cord. The axonal damage in the spinal cord was less severe compared with that observed in nerve fibers associated with DRGs (dorsal nerve root and spinal nerve).

While the severity of neuron and nerve fiber degeneration was comparable between the two species, inflammation was more prominent

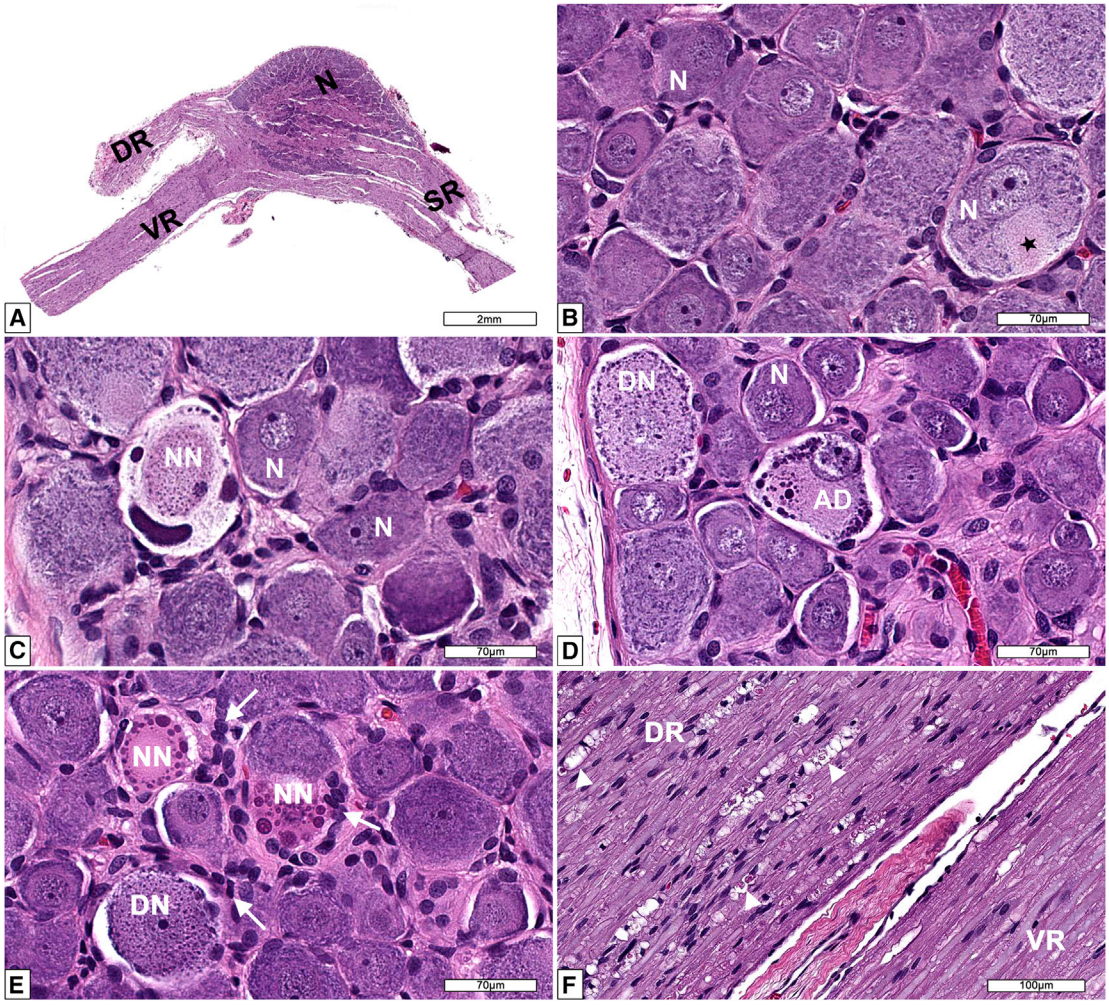

Figure 1. Microscopic findings in dorsal root ganglia (DRG) from AAV-treated Wistar Han rats

(A) Low magnification and (B) high magnification of the dorsal root ganglion (DRG) and spinal roots at lumbar 4 (L4) spinal cord segment from a male 12-week-old control Wistar Han rat. DR = dorsal spinal nerve root composed of somatic and autonomic nerve fibers (ascending sensory information passing to central nervous system); N = neurons forming the DRG and normal axon hillock (black star); SR = spinal nerve containing both sensorimotor and autonomic nerve fibers; VR = ventral spinal nerve root composed of motor and autonomic nerves (descending motor information arising from the CNS). (C) DRG L4 of a male Wistar Han rat administered 1×10^{14} vg/kg of AAV showing a neuron undergoing necrosis (NN) characterized by dense basophilic round to elongated structures displaced to the periphery (nucleus and Nissl body) and central an oval eosinophilic granular material (cytoplasmic structures). (D) DRG thoracic 3 from a male Wistar Han rat administered 1×10^{14} vg/kg of AAV depicting normal neurons (N) and affected neurons undergoing degeneration (DN) and another degenerated neuron showing atypical chromatolysis (AD) (cell with eccentric nucleus and eosinophilic cytoplasm with marginated Nissl bodies that formed large lumping and globular structures). (E) DRG L4 from a male Wistar Han rat administered 5×10^{13} vg/kg of AAV showing reactive (hyperplastic/hypertrophic) satellite glial cells and activated macrophages (white arrows). A neuron undergoing degeneration (DN) and necrotic neurons (NN). (F) Nerve roots of DRG L4 from a male Wistar Han rat administered 1×10^{14} vg/kg of AAV showing nerve fiber degeneration (*white arrowheads*) in the dorsal nerve root (DR) while the ventral nerve root (VR) is unremarkable. Processing: Neutral buffered 10% formalin (NBF)-fixed, paraffin embedded, H&E-stained sections.

in the cynomolgus monkeys compared with the rats. Mild to moderate mononuclear cell infiltration was observed in monkeys exhibiting neuron/nerve fiber degeneration. In a similar monkey study, minimal focal to multifocal mononuclear cell infiltrate and reactive satellite glial cells were observed around necrotic neurons (shrunken neurons/neuronophagy) as early as day 5 post treatment at $\geq 5 \times 10^{13}$ vg/kg,[12] suggesting inflammation may directly contribute to the mechanism of toxicity in this species. In contrast, the minimal to mild mononuclear cell infiltration and glial cell hypertrophy observed in rats was likely a secondary response initiated to resolve the damaged neurons. The DRG and spinal cord lesions from this rat study and a similar cynomolgus monkey study have been comprehensively characterized in a previous publication, which includes regional differences in histologic findings and immunohistochemical profiling of mononuclear cell infiltrates.[12]

Table 2. Group incidence and severity of dorsal root ganglia microscopic findings in male cynomolgus monkeys

Dose (vg/dose)	3.0×10^{13}	3.3×10^{13}	8.7×10^{13}
Number of injections	1	3	1
n per group	2	2	2
Neuron degeneration/necrosis	0	1	2
Minimal (Grade 1)	0	0	0
Mild (Grade 2)	0	1	1
Moderate (Grade 3)	0	0	1
Nerve fiber degeneration	0	1	2
Minimal (Grade 1)	0	1	1
Mild (Grade 2)	0	0	0
Moderate (Grade 3)	0	0	1
Mononuclear cell infiltration	2	1	2
Minimal (Grade 1)	2	0	0
Mild (Grade 2)	0	1	1
Moderate (Grade 3)	0	0	1

Prioritization of cell-specific candidate biomarkers

To evaluate cross-reactivity against various species of interest, antibodies against each candidate biomarker were tested on brain lysate from human, cynomolgus monkey, rat, and mouse via capillary electrophoresis (ProteinSimple, Wes). Antibodies were also tested against monkey and rat DRG lysate to determine whether the candidate is present in this tissue. Both the capture and detection antibodies for UCH-L1 cross-reacted well with all four species tested. Moreover, UCH-L1 signal detected in monkey and rat DRGs was comparable to the brain (Figure 3). Interestingly, NF-L detection exhibited substantial variability both within and between species. NF-L was higher in rat DRGs compared with rat brain, while monkey NF-L was similar between the two tissues. In human and mouse brain, the NF-L detection antibody yielded a stronger signal compared with the capture antibody (Figure 3). For CNPase and IBA1, antibody cross-reactivity and presence in DRGs were confirmed for each species tested (Figure S1A and S1B). Glial fibrillary acidic protein (GFAP) was not detected in DRGs from either rat or monkey despite confirmation of cross-reactivity using brain and/or serum (Figure S1C). Although the mouse total Tau R-PLEX antibodies exhibited good cross-reactivity with rat brain, little to no signal was detected in rat DRGs. For the human total Tau R-PLEX kit, only the capture antibody exhibited cross-reactivity with monkey brain, while neither antibody detected appreciable signal in monkey DRGs (Figure S1D). Therefore, neither GFAP nor total Tau were considered promising candidates for monitoring DRG toxicity. Given the large molecular weight of MAP2 (~280 kDa), it is unlikely that the full-length protein would be released into circulation following moderate neurodegeneration. The presence of smaller MAP2 degradation products was therefore evaluated in serum and CSF, revealing 50 to 63 kDa fragments in both monkey and rat (Figure S1E). Although this demonstrates feasibility for monitoring MAP2 as a non-invasive circulating biomarker, further characterization of the serum and CSF fragments would be required to synthesize an appropriate protein standard.

Our seven candidate biomarkers were prioritized based on the factors described above. UCH-L1 and NF-L emerged as the top candidates given the availability and cross-reactivity of the Meso Scale Discovery (MSD) R-PLEX kits. CNPase, IBA1, and MAP2 were classified as a lower priority given the commercially available antibodies require conjugation to biotin and the MSD SULFO-TAG. MAP2 was further deprioritized due to the added complexity of characterizing the circulating fragments. GFAP and total Tau were excluded due to their low/undetectable levels in DRGs. It is important to note that protein expression was evaluated in brain and DRG samples from naive animals. Given that AAV treatment may alter the tissue-specific profiles of these candidates, GFAP and total Tau levels should be examined in the DRGs of AAV-treated animals before ruling out their potential use as biomarkers. The remainder of this article focuses on our top biomarker candidates: NF-L and UCH-L1.

MSD assay validation

Using rat plasma as the biological matrix of interest, the duplex MSD assay underwent a "fit-for-purpose" validation, successfully passing each of the following tests: 1) intra-assay accuracy and precision, 2) inter-assay accuracy and precision, 3) freeze-thaw stability, and 4) dilution linearity. More specifically, quality control (QC) samples in rat plasma exhibited coefficient of variation values (CVs) $\leq$25% between replicates (intra-assay) and plates (inter-assay), where the bias between observed and expected values was within 25%. For NF-L, the analytical lower and upper limits of quantitation (LLOQ, ULOQ) were determined to be 24 and 25,000 pg/mL, while the quantitative range for UCH-L1 was determined to be 391 to 400,000 pg/mL (Table S1). For each plate, the MSD software defines the lower limit of detection (LOD) as 2.5 SDs above the blank. Considering the values across each validation plate, the average analytical LOD for NF-L and UCH-L1 was 7.37 and 213 pg/mL, respectively. The functional sensitivity parameters for samples diluted 4- or 6-fold are listed in Table S1. Compared with the initial thaw of the QC samples, 75% to 125% recovery was obtained following up to four freeze/thaw cycles at −80°C. Moreover, serial dilutions of 2- to 64-fold in rat plasma demonstrated linearity with a coefficient of determination (R^2) above 0.9.

Following the full "fit-for-purpose" validation in rat plasma, bridging validations were performed for additional biological matrices. Intra-assay precision and accuracy, as well as dilution linearity, were confirmed for both analytes in rat and monkey CSF. In rat serum and monkey serum/plasma, only NF-L passed the bridging validation, while the bias between observed versus expected UCH-L1 values fell outside the acceptable limits. Specifically, observed values of UCH-L1 were more than 30% lower than expected, suggesting these matrices substantially suppress detection of this analyte. Table S2 summarizes the validation results for each biological matrix evaluated. A bridging validation was also performed for the singleplex version of the NF-L assay. In a side-by-side comparison on a single plate, CVs between the

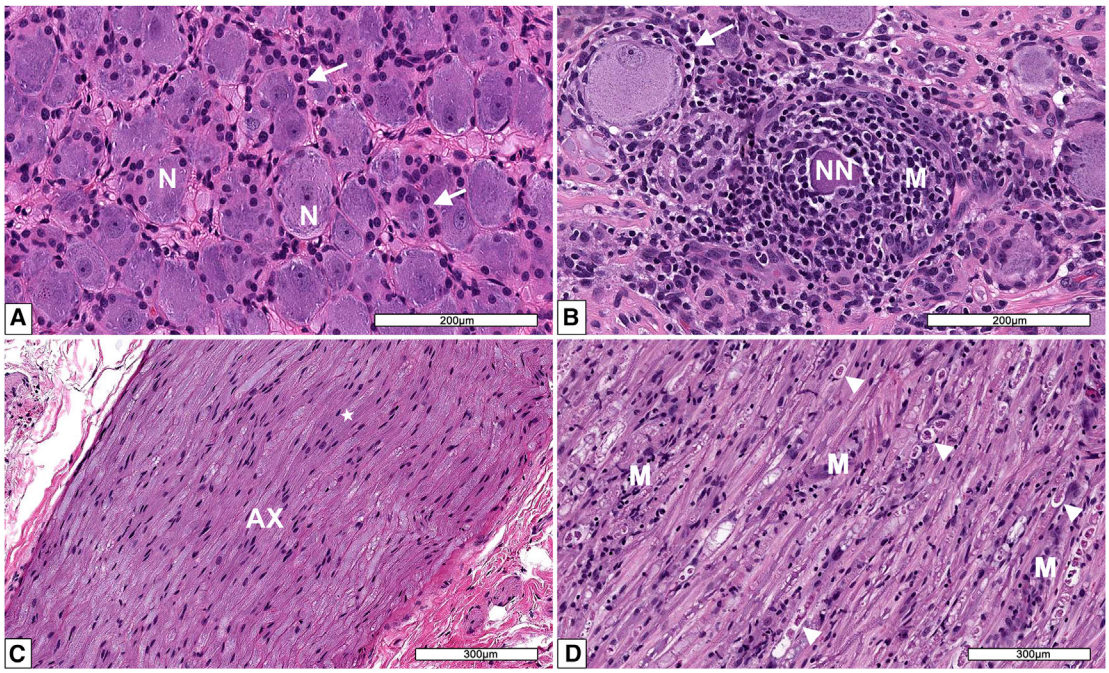

Figure 2. Microscopic findings in dorsal root ganglia (DRG) from AAV-treated cynomolgus monkeys

(A) DRG from a male control monkey depicting healthy neurons (N) and numerous satellite glia cells (*white arrows*). (B) DRG from a monkey administered a single injection of 8.7×10^{13} vg per animal intrathecally. A necrotic neuron (NN) is surrounded by many mononuclear cells (M). Reactive (hyperplasia/hypertrophy) satellite glial cells surround a normal neuron. (C) Dorsal nerve root from a DRG of a male control monkey composed of axons (AX) surrounded by Schwann cells (*white star*). (D) Dorsal nerve root from a DRG of a monkey administered a single injection of 8.7×10^{13} vg per animal intrathecally. Multiple *arrowheads* depict nerve fibers undergoing nerve fiber degeneration characterized by dilated myelin sheaths containing fragmented myelin and axons. Schwann cell reactivity and infiltration of mononuclear cells (M) are also evident. Processing: Neutral buffered 10% formalin (NBF)-fixed, paraffin embedded, H&E-stained sections.

singleplex versus duplex versions were less than 5% for each NF-L standard and QC sample.

NF-L in AAV-treated rats and cynomolgus monkeys

To investigate whether NF-L or UCH-L1 values were associated with DRG toxicity in rats, plasma from AAV-treated rats was analyzed using our in-house duplex MSD assay. Compared with vehicle, NF-L values were time- and dose-dependently increased in animals treated with $\geq 5 \times 10^{13}$ vg/kg AAV (Figures 4A and 4B). In rats that exhibited DRG toxicity, NF-L was increased 9.7- and 18.7-fold on study day 8 and 29, respectively, compared with animals with no remarkable treatment-related histologic findings (Figures 4C and 4D). Considering the histologic scores for each DRG finding, NF-L was strongly associated with the severity of both DRG neuron degeneration/necrosis (Figures 4E and 4F) and nerve fiber degeneration of DRG nerve roots (Figures 4G and 4H). In animals with mild neuronal degeneration and/or moderate nerve fiber degeneration, NF-L was increased as early as 8 days following AAV treatment, while animals with minimal neuron degeneration and/or mild nerve fiber degeneration exhibited an increase on day 29. On day 29, NF-L values were below the functional LLOQ (96 pg/mL) in animals with no remarkable histologic findings, while all animals with mild or moderate neuron-specific findings (neuron degeneration and/or nerve fiber degeneration) exhibited values above 300 pg/mL. Mononuclear cell infiltration and glial cell hypertrophy were weakly associated with NF-L compared with neuron-specific toxicity. Interestingly, three rats exhibited elevated NF-L on day 4. NF-L then returned to and remained at baseline by day 8 and 29, consistent with the lack of remarkable DRG lesions in these animals (Figure 4D).

Serum samples from AAV-treated cynomolgus monkeys were also analyzed using the duplex MSD assay. On day 29, monkeys with DRG toxicity ($\geq 3.3 \times 10^{13}$ vg/dose) exhibited a trending 4.2-fold increase in serum NF-L compared with animals with no remarkable DRG findings, with elevations beginning on day 14 in one animal (Figures 5C and 5D). The lack of statistical significance is not surprising given the small number of animals used in the study. Consistent with the rat results, monkey serum NF-L was associated with the severity of DRG neuron degeneration/necrosis (Figures 5E and 5F) and nerve fiber degeneration of DRG nerve roots (Figures 5G and 5H). However, one monkey exhibited relatively high serum NF-L on day 29 despite no remarkable DRG findings. It is possible this animal sustained procedure-related neurological injury during implantation of the intrathecal catheter, as previously reported.[29] CSF samples from 5 of 6 monkeys on day 29 were also analyzed; insufficient volume was available from one animal which received 3.3×10^{13} vg/dose [3x]. A monkey with mild neuron degeneration and minimal nerve fiber degeneration exhibited

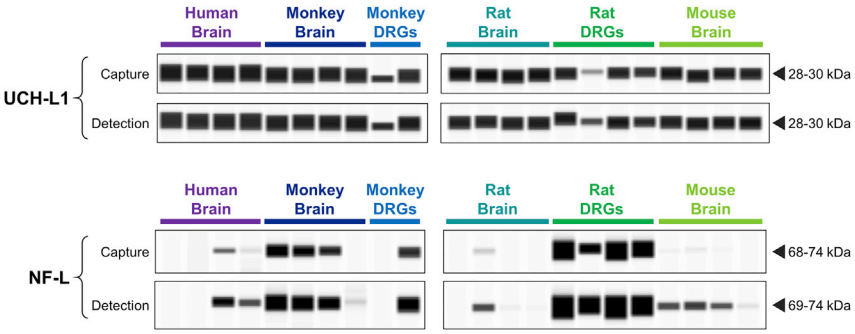

Figure 3. Detection of UCH-L1 and NF-L in brain and dorsal root ganglia (DRG) from nonclinical species

Wes capillary electrophoresis (ProteinSimple) was used to confirm cross-reactivity of the capture and detection antibodies within MSD R-PLEX kits for human UCH-L1 (F211O) and human NF-L (F217X). Each antibody was tested against brain homogenate (n = 4) from human, cynomolgus monkey, Wistar Han rat, and CD1 mouse. Dissected DRGs from monkey (n = 2) and rat (n = 4) were also assessed. Chemiluminescence signals were analyzed with Compass software (ProteinSimple), where image contrast was adjusted separately for each antibody to visualize the presence versus absence of the target peak.

substantially higher NF-L in CSF compared with the other animals (Figure S2). However, CSF NF-L from the animal with the most severe DRG toxicity (moderate neuron and nerve fiber degeneration) was comparable to animals exhibiting no DRG toxicity. Based on these results, serum and plasma were determined to be the optimal matrices for measuring NF-L as a biomarker of DRG toxicity rather than CSF.

Serum/plasma NF-L was also compared against the histologic lesions in the spinal cord (ascending sensory axons with cell bodies in the DRGs). In both species, NF-L was strongly associated with the severity of spinal cord nerve fiber degeneration (Figures S3A and S3B). Notably, the correlation coefficient between NF-L versus nerve fiber degeneration severity in the spinal cord of rats (Figure S3D; R^2 = 0.7463) was comparable to that for the DRGs (Figure S3C; R^2 = 0.7571). However, the axonal damage associated with the DRGs was more severe than the nerve fiber degeneration observed in the spinal cord.

UCH-L1 in AAV-treated rats and cynomolgus monkeys

Throughout the study period, plasma UCH-L1 values were below the functional LLOQ (1.56 ng/mL) in all rat samples, with most samples also falling below the detection limit (data not shown). Similarly, UCH-L1 values in serum and CSF were below the functional LLOQ (2.35 ng/mL) in five of six monkeys, although the outliers in each matrix were not the same animal. The single monkey with quantifiable serum UCH-L1 received the lowest dose (3.0×10^{13} vg/dose [1x]) and exhibited no DRG toxicity, while the monkey with quantifiable CSF UCH-L1 exhibited mild DRG neuron degeneration with minimal nerve fiber degeneration (Figures S4 and S5).

Characterization of baseline NF-L in naive animals

Given that NF-L demonstrated promise as a circulating biomarker of DRG toxicity, baseline serum and plasma profiles were characterized in age-matched naive rats (n = 18) and cynomolgus monkeys (n = 20) using the singleplex version of the assay. In male rats, the average NF-L value in plasma (35.5 pg/mL) was significantly higher than in serum (24.7 pg/mL). Similarly, the average NF-L value in female rats was higher in plasma (44.1 pg/mL) compared with serum (38.2 pg/mL), although this difference failed to reach significance (p = 0.065) (Figure 6A). All but one of the rats exhibited plasma NF-L below the functional LLOQ (96 pg/mL), with most animals falling between the LOD and LLOQ of the assay. In monkeys, serum and/or plasma NF-L was below the LOD in 17 of the 20 animals, while only one animal exhibited values close to the functional LLOQ (144 pg/mL) (Figure 6C). No statistically significant differences in NF-L were observed between sexes in either species. Moreover, NF-L values between plasma and serum were highly correlated in both rats and monkeys, with a coefficient of determination (R^2) above 0.9 (Figure 6B and 6D).

MSD versus Quanterix platform comparison

To compare the performance of our in-house MSD assay against a commercially available bead-based NF-L assay, the rat plasma and monkey serum/CSF samples from day 29 were analyzed on the Quanterix Simoa HD-X. The resulting Quanterix data were highly correlated with our in-house MSD values for both rat and monkey, with R^2 values of 0.979 and 0.996, respectively (Figures S6B and S6D). In rat plasma, the NF-L values determined via MSD were approximately 2-fold greater than the Quanterix values, while the MSD values for monkey serum and CSF were approximately 3-fold greater than Quanterix (Figures S6A and S6C). The sensitivity of the Quanterix HD-X assay was superior to that of the MSD assay, with an analytical LLOQ of 0.5 pg/mL compared with 24 pg/mL.

DISCUSSION

DRG toxicity observed in preclinical studies of AAV gene therapy has triggered the need for more rigorous risk assessment prior to initiation of clinical trials. During the recent meeting held by the U.S Food and Drug Administration's Cellular, Tissue, and Gene Therapies Advisory Committee (https://youtu.be/yLggQF0XUUY), a clear consensus emerged among panelists regarding a paucity in our current toolkit for evaluating DRG toxicity and the critical need for non-invasive safety biomarkers. Our studies address this key knowledge gap and help advance the DRG risk assessment strategies for AAV vectors.

In these studies, our top tier biomarker candidates (NF-L and UCH-L1) were temporally monitored in rats and cynomolgus monkeys following AAV treatment and then compared with terminal histologic DRG findings on day 29. In rats and monkeys exhibiting DRG toxicity, blood NF-L was elevated as early as days 8 and 14, respectively. In the rat study, a separate cohort exhibited no remarkable

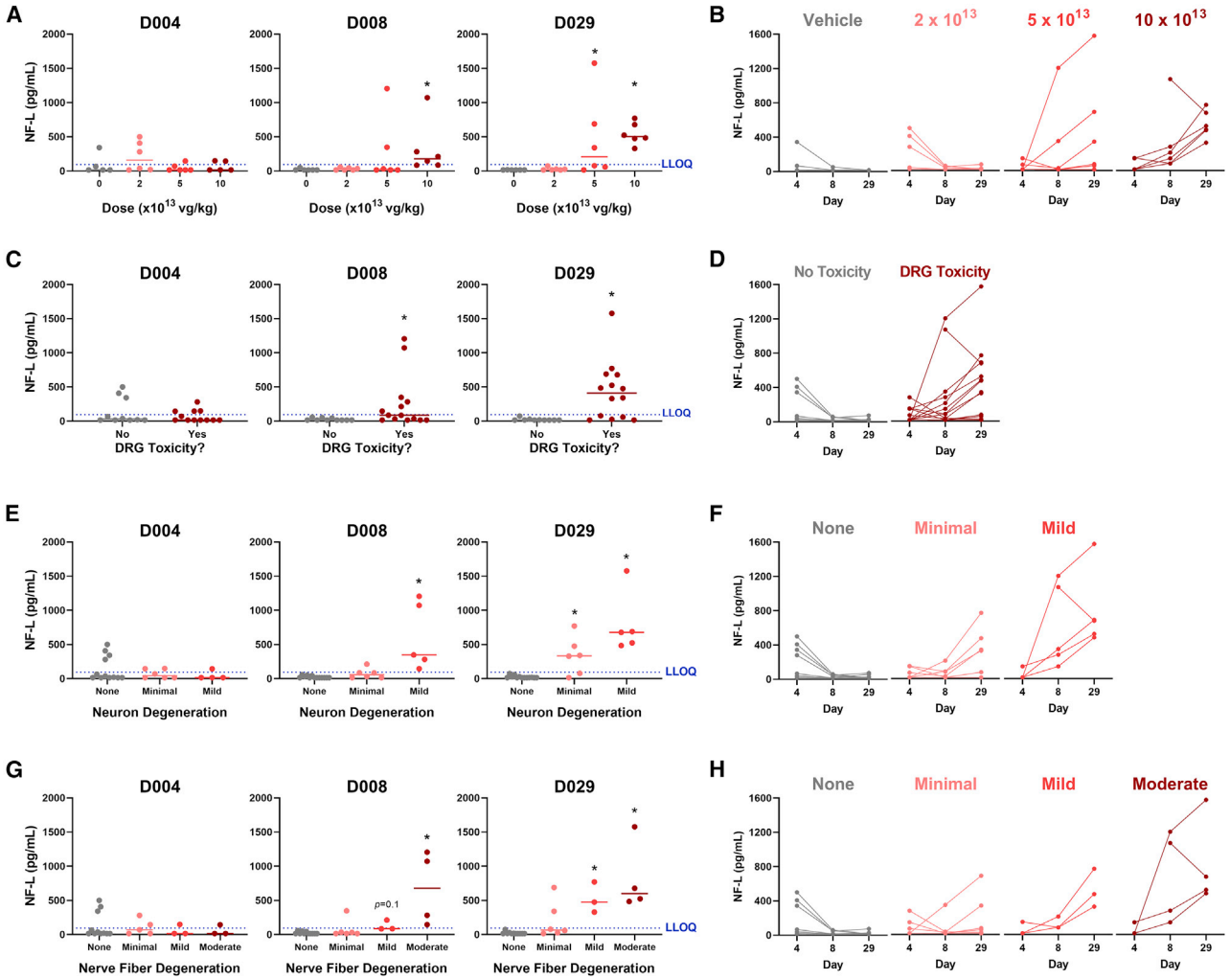

Figure 4. Plasma NF-L is elevated in rats exhibiting AAV-induced dorsal root ganglia (DRG) neurotoxicity

Male Wistar Han rats (n = 6) were intravenously injected with a bolus dose of 0, 2×10^{13}, 5×10^{13}, or 1×10^{14} vg/kg AAV vector. Plasma was collected 4, 8, and 29 days after injection, while histologic DRG lesions were assessed on day 29. NF-L in plasma was quantified using an in-house duplex MSD assay. For each study day, NF-L was plotted against (A) AAV dose, (C) presence/absence of DRG toxicity (neuronal and/or nerve fiber degeneration), (E) severity of DRG neuron degeneration/necrosis, and (G) severity of DRG nerve fiber degeneration. The dashed blue line indicates the lower limit of quantification (LLOQ = 96 pg/mL). Statistical significance (*$p \leq 0.05$) was evaluated through a Kruskal-Wallis test followed by Dunn's multiple comparison test (A, E, and G) or Welch's t test (C) performed in GraphPad Prism 9.0.0. The NF-L profile for each animal has also been plotted by (B) AAV dose, (D) presence/absence of DRG toxicity (neuronal and/or nerve fiber degeneration), (F) severity of DRG neuron degeneration/necrosis, and (H) severity of DRG nerve fiber degeneration. Any values which fell below the limit of detection (LOD) were plotted as the functional LOD for that plate.

DRG lesions 4 days after AAV treatment.[12] A more extensive time course study will be required to determine whether elevations in blood NF-L can be detected prior to development of overt microscopic lesions, informing the predictive value of this biomarker. Moreover, understanding when circulating NF-L returns to baseline following remission of DRG neuronal degeneration will be important for risk assessment in humans. In patients with neurosurgical CNS trauma[30] and oxaliplatin-induced peripheral neuropathy,[31] increased serum NF-L returned to baseline after 6 to 9 months suggesting NF-L elevations associated with DRG toxicity may be detectable well beyond 1 month. Any future translation of serum NF-L as a biomarker of AAV-induced DRG neurotoxicity in humans will require a better understanding of the relation between the time course of neurotoxicity and elevated serum NF-L.

Circulating NF-L in naive animals, as well as vehicle- and AAV-treated animals lacking DRG toxicity, lie within a narrow range. The low biological variability in baseline NF-L enabled the biological sensitivity of this biomarker, where statistically significant elevations were detected in animals with low-grade histologic lesions including minimal (grade 1) neuron degeneration and mild (grade 2) nerve fiber degeneration. As expected, the association between blood NF-L

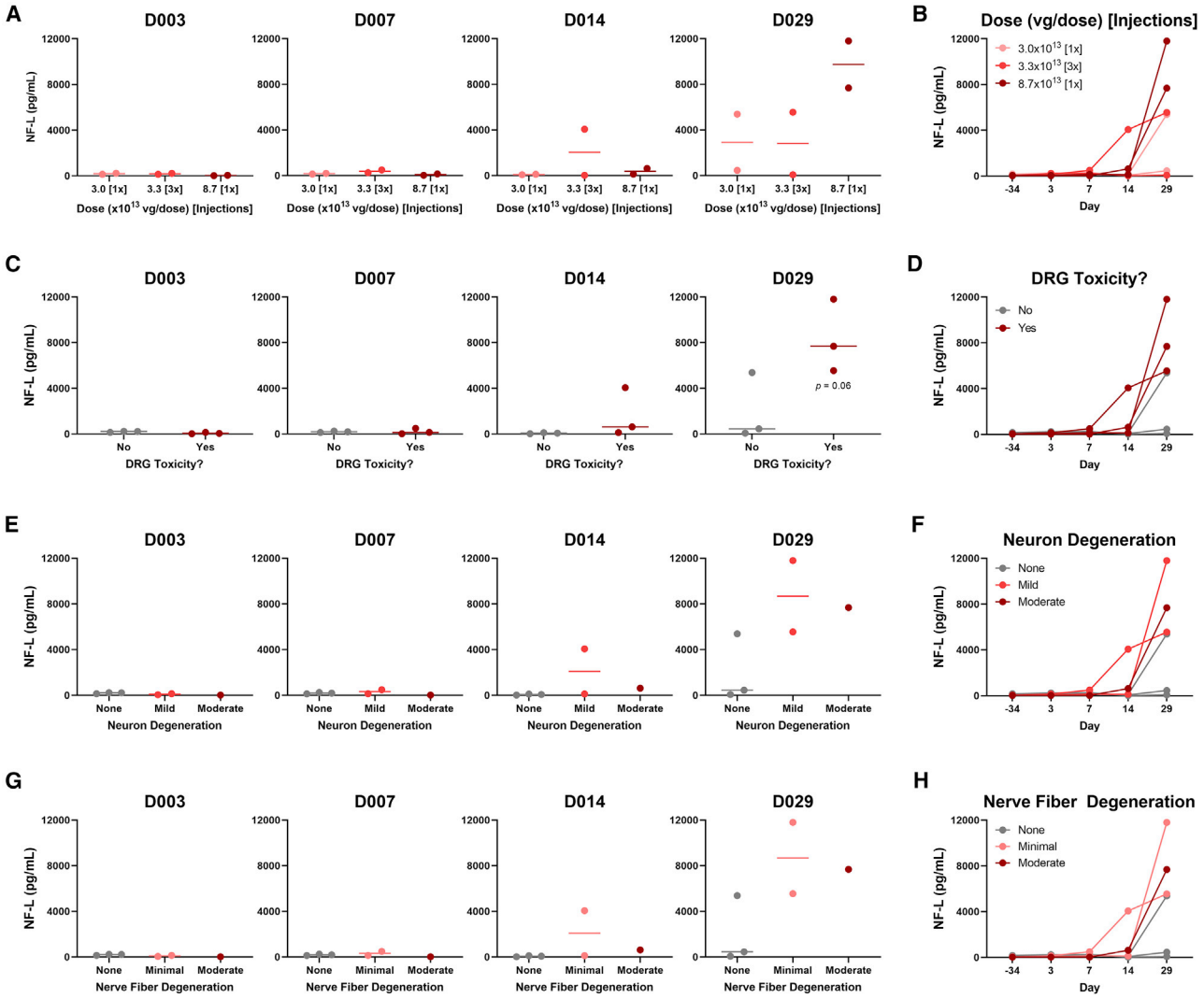

Figure 5. Serum NF-L is elevated in cynomolgus monkeys exhibiting AAV-induced DRG neurotoxicity

Male cynomolgus macaques (n = 2) were injected with 3.0×10^{13} [1x], 3.3×10^{13} [3x], or 8.7×10^{13} [1x] vg/dose AAV vector via intrathecal catheter. Serum was collected 3, 7, 14, and 29 days after injection, while histologic DRG lesions were assessed on day 29. NF-L in serum was quantified using an in-house duplex MSD assay with a functional lower limit of quantification (LLOQ) of 144 pg/mL. For each study day, NF-L was plotted against (A) AAV dose, (C) presence/absence of DRG toxicity (neuronal and/or nerve fiber degeneration), (E) severity of DRG neuron degeneration/necrosis, and (G) severity of DRG nerve fiber degeneration. Statistical significance ($p \leq 0.05$) was evaluated through one-way ANOVA analysis followed by Dunnett's multiple comparison test (A, E, and G) or t test (C) performed in GraphPad Prism 9.0.0. The NF-L profile for each animal has also been plotted by (B) AAV dose, (D) presence/absence of DRG toxicity (neuronal and/or nerve fiber degeneration), (F) severity of DRG neuron degeneration/necrosis, and (H) severity of DRG nerve fiber degeneration. Any values which fell below the limit of detection (LOD) were plotted as the functional LOD for that plate.

and severity of neuron/nerve fiber degeneration was stronger than the association with either mononuclear cell infiltration or glial cell hypertrophy. It is well known that neurofilaments such as NF-L are expressed primarily in the axon of a neuron, and thus glial cells do not contribute directly to the circulating neurofilament pool.[32] This restricted expression profile makes NF-L a highly specific marker of neuroaxonal degeneration, reducing the risk of false positives.

To our knowledge, this is the first study to demonstrate the use of NF-L as a circulating biomarker of DRG-related neurotoxicity. However, previous studies report increased NF-L in rats treated with various neurotoxicants (e.g., chloropropionic acid, acrylamide, trimethyltin, kainic acid), as well as rodent models of Huntington's disease and pneumococcal meningitis.[33–36] Moreover, circulating NF-L was elevated in patients with traumatic brain injury (TBI)[37–39] and several neurodegenerative diseases including multiple sclerosis, Alzheimer's disease, ALS, spinal muscular atrophy, and Guillain-Barré syndrome.[40–43] In each of these studies, NF-L was elevated in CSF as well as blood-derived biofluids. Notably, in our monkey study, NF-L in CSF was weakly associated with DRG toxicity

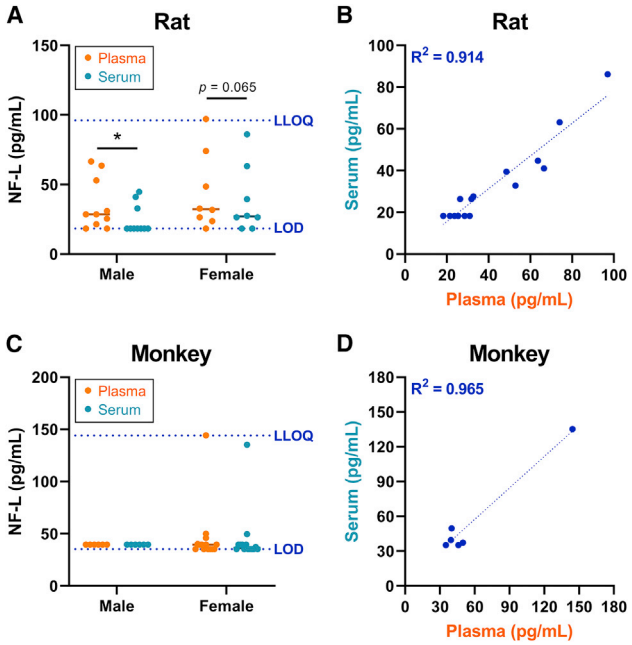

Figure 6. Characterization of baseline NF-L values in naive rats and cynomolgus monkeys

An in-house singleplex MSD assay was used to quantify NF-L in matched plasma and serum from naive (A) Wistar Han rats and (C) cynomolgus macaques. The dashed blue lines indicate the functional limit of detection (LOD) and lower limit of quantification (LLOQ). Statistical significance (*p $\leq$ 0.05) was evaluated through two-way ANOVA analysis followed by Sidak's multiple comparisons test (A and C) performed in GraphPad Prism 9.0.0. The correlation between plasma and serum values of NF-L is shown for (B) rats and (D) monkeys, where the coefficient of determination (R^2) was determined through linear regression analysis. Any values that fell below the limit of detection (LOD) were plotted as the functional LOD for that plate.

compared with serum. This is consistent with the anatomy of DRGs, which lie outside the blood-brain barrier and are surrounded by only a thin layer of CSF.[44] Moreover, the interface between DRGs and blood vessels is highly unique, where fenestrated capillaries readily irrigate sensory neurons with a robust supply of blood to fulfill their metabolic needs.[44–47] Blood-borne molecules can easily enter DRG neurons, and in turn, DRG-derived molecules are released directly into circulation. This unique anatomy, combined with our comparison of monkey NF-L across matrices, suggest NF-L changes in blood-derived biofluids (serum, plasma) might reflect DRG toxicity better than CSF. Although the correlations between NF-L versus nerve fiber degeneration in the DRGs and spinal cord were comparable, the axonal damage in nerve fibers associated with DRGs (dorsal nerve root and spinal nerve) was more severe than that observed in the spinal cord. Therefore, the majority of circulating NF-L was likely derived from nerve fiber degeneration within the peripheral nervous system (PNS; including the DRGs), rather than the spinal cord. However, the contribution of the CNS to circulating NF-L through CSF cannot be excluded. In summary, NF-L is a versatile biomarker for both CNS and PNS neurotoxicity, although the ideal matrix for analysis may depend on the specific neurons targeted.

Prior to biomarker analysis, the presence of UCH-L1 protein in rat and monkey DRGs was confirmed through capillary electrophoresis, with levels comparable to the brain. However, regardless of AAV treatment or DRG toxicity, plasma UCH-L1 fell below the functional LLOQ in all rat plasma samples and all but one monkey serum sample analyzed. The utility of UCH-L1 as a nonclinical biomarker of AAV-induced DRG toxicity therefore remains unclear as it is possible our in-house assay simply lacks the sensitivity required to detect modest changes. Interestingly, a time course analysis of UCH-L1 in a rat model of TBI found serum values peaked between 2 and 6 h following cortical impact, with values approaching baseline 36 h after injury.[48] Similarly, UCH-L1 CSF from TBI patients were reported to peak 6 h following concussion and then decrease over time.[49] Following AAV treatment, the earliest timepoints evaluated in our monkey and rat studies were 72 and 96 h, respectively, and thus evaluating serum UCH-L1 at an earlier time point would be worthwhile. However, a biomarker that is only transiently increased following treatment may be difficult to reliably detect, monitor, and compare across subjects. Compared with the short half-life of UCH-L1,[50] NF-L is stable in both blood and CSF for weeks to months, allowing for flexibility in the blood collection timeline.[30]

CNPase, IBA1, and MAP2 were identified as promising candidates for evaluating the role of oligodendrocytes, macrophages/microglia, and neuronal dendrite alterations, respectively, in DRG toxicity. However, additional studies are needed to examine whether blood concentrations of these candidates correlate with AAV-elicited histologic findings. It is important to note that IBA1 is expressed by all macrophages throughout the body and thus it would be difficult to distinguish microglia activation from other AAV-induced pathologies such as immunogenicity and hepatotoxicity. MAP2 has proven valuable for assessing dendrite-specific neuronal injury via immunohistochemistry.[51–53] Due to its large size, however, it is unlikely that the full-length version (~280 kDa) of this protein would be present in circulation. We detected small MAP2 fragments (50-63 kDa) in serum and CSF from naive rats and cynomolgus monkeys. This is consistent with previous studies that report 50 and 70 kDa MAP2 fragments in serum from rats following ischemia/reperfusion injury[54] and humans with bipolar depression,[55] respectively. The presence of small MAP2 fragments in easily accessible bodily fluids confirms the feasibility of using this candidate as a non-invasive biomarker of neuronal dendrite injury.

In conclusion, NF-L is a sensitive blood-based biomarker of DRG toxicity that can be used to non-invasively assess AAV-induced neurotoxicity in rats and cynomolgus monkeys. Blood levels of NF-L were increased even with mild to moderate DRG neurotoxicity, suggesting greater sensitivity than other in-life measures including behavioral changes and neurophysiological assessments (e.g., nerve conduction velocity [NCV], sensory nerve action potential [SNAP]). In NHPs with AAV-induced DRG toxicity, NCV assessments revealed changes at a low frequency and only in the most severely affected animals.[22] Moreover, the translational value of NF-L exhibits great promise, where blood values could be used to

manage risk for AAV-induced DRG toxicity in human clinical trials. Notably, age-dependent reference values of serum NF-L have been determined in healthy adults, demonstrating elevated and more variable levels above 60 years of age.[56,57] In addition, elevated serum NF-L is reported to be predictive of chemotherapy-induced peripheral neuropathy.[31,58] The Innovative Medicines Initiative (IMI) Translational Safety Biomarker Pipeline (TransBioLine) project includes a workstream to qualify serum NF-L, along with other nervous system-derived proteins, as biomarkers of drug-induced CNS injury in humans.[59,60] Although these developments are encouraging, further research is needed to understand human serum profiles of NF-L before it can be implemented in AAV clinical trials. Specifically, it will be important to determine how pre-existing neurological diseases affect detection of AAV-induced NF-L changes in patients receiving gene therapy.[43,61] Once further characterized across diverse human populations, this sensitive biomarker of DRG toxicity could become a fundamental tool for monitoring the safety of novel AAV-delivered therapeutics.

MATERIALS AND METHODS

Animal procedures

Studies were conducted in accordance with the current guidelines for animal welfare (National Research Council Guide for the Care and Use of Laboratory Animals, 2011 and Animal Welfare Act [AWA], 1966, as amended in 1970, 1976, 1985, and 1990, and the AWA implementing regulations in Title 9, Code of Federal Regulations, Chapter 1, Subchapter A, Parts 1-3). The procedures used in these studies have been reviewed and approved by Pfizer's Institutional Animal Care and Use Committee.

The two studies reported in this article were not specifically designed to investigate the underlying mechanism of AAV-mediated DRG toxicity. The rat study was conducted to determine whether the AAV-mediated hepatic and DRG neuronal toxicity reported by others following intravenous administration in rhesus monkeys[13] could be reproduced in a rodent model.[12] The monkey study was conducted for a proprietary gene therapy candidate in Pfizer's pipeline, and thus the route of administration was selected based on program-specific considerations.

A total of 24 male Wistar Han (Crl:WI[Han]) rats were acclimated to the facility for a minimum of 5 days prior to initiation of dosing and were aged 7 to 9 weeks at study start. Animals were singly housed in individually ventilated cages from receipt through a Biosafety Level-2 period and in suspended cages for the rest of the study duration. Rats were allocated to study groups using a computer-assisted randomization procedure based on pre-dose body weights. Dosing formulations for each group were prepared by diluting the stock test article in a vehicle consisting of 0.002% Pluronic F68 in 10 mM Phosphate, 350 mM NaCl, 2.7 mM KCl, 5% Sorbitol in sterile water (pH 7.4). Rats (n = 6 per dose group) received a single bolus of an AAV9 variant vector (AAV-PHP.b) at 0, 2×10^{13}, 5×10^{13}, or 1×10^{14} vg/kg, administered through intravenous injection via the caudal vein of the tail. This neurotropic variant vector expressed the human survival motor neuron 1 (*SMN1*) transgene driven by the ubiquitous CBh (hybrid form of chicken Beta actin) promoter (AAV-PHP.b-CBh-SMN1) as previously described.[12] Clinical observations were recorded after the last animal was dosed on day 1 and twice daily on non-dosing days. All rats were fasted overnight prior to necropsy and were euthanized on day 29. To analyze circulating biomarkers, blood was collected in K_2EDTA VACUETTE tubes (Greiner Bio-One, Monroe, NC) on days 4, 8, and 29 post-dosing. Blood was centrifuged at 2,500 × *g* for 10 min to separate plasma.

A total of six male cynomolgus macaques of Mauritius origin aged ≥2.5 years at initiation of dosing were socially housed and acclimated to the laboratory environment. All animals selected for the study were seronegative (titer ≤1:5) for neutralizing antibodies against the AAV9 capsid to ensure unaltered tissue transduction. Animals were implanted with an intrathecal catheter in the lumbar area with a subcutaneous access port for dosing and CSF collection. Animals were sedated and placed in the Trendelenburg position with the head tilted down 15 to 30° below the pelvis for dose administration and kept in this position for approximately 15 min post-dose. Cynomolgus monkeys (n = 2 per dose group) were administered a proprietary AAV9 vector by slow injection (over approximately 2 min) via intrathecal catheter port according to the following dosing regimens: (1) three injections of 3.3×10^{13} vg, with the second and third injection administered approximately 6 and 24 h after the first injection (total dose = 1.0×10^{14} vg/animal), (2) single injection of 8.7×10^{13} vg, or (3) single injection of 3.0×10^{13} vg. Dosing formulations were prepared using the same vehicle described above. Immediately after administration, the catheter was flushed with 0.5 mL artificial CSF. On dosing days, clinical observations were recorded prior to injection, ≤2 h after the last animal was dosed, and at the end of the workday; on non-dosing days, clinical observations were recorded twice daily. Monkeys were fasted overnight prior to necropsy and were euthanized on day 29 post-dosing. To analyze circulating biomarkers, blood was collected in Serum Separator Clot Activator VACUETTE tubes (Greiner Bio-One) on Pre-Dose day 34 and days 3, 7, 14, and 29 post-dose. Blood was centrifuged at 2,500 × *g* for 10 min to separate serum. CSF was collected on day 1 (pre-dose) and 29 (post-dose).

While only male rats and monkeys were included in these AAV studies, it has previously been shown that AAV-induced DRG toxicity affects males and females equally.[22] To characterize baseline biomarker profiles in age-matched naive animals, plasma and serum samples were collected from 18 naive Wistar Han rats (8 females, 10 males) and 20 naive cynomolgus monkeys (14 females, 6 males).

AAV vectors

AAV vectors were purified in HEK293 cells grown in suspension media after triple transfection with packaging plasmid (rat study: PHP.b; monkey study: AAV9) and adenovirus helper plasmid. Triple transfected cells were lysed, crude lysate was cleared, and vectors were purified from an affinity column followed by IOD gradient separation. Finally, vectors were polished using Cation Exchange

Table 3. Biomarker selection and prioritization based on reagent availability, cross-reactivity, and detection in dorsal root ganglia

		Reagent availability			Cross-reactivity		Detected in DRGs
Biomarker	Cell type specificity	MSD R-plex kit	Antibodies	Protein standard	Monkey	Rat	
UCH-L1	Neurons	F211O (human)	Included in kit	Included in kit	Yes	Yes	Yes
NF-L	Neurons (axons)	F217X (human)	Included in kit	Included in kit	Yes	Yes	Yes
IBA1	Microglia	Not available	Abcam (ab178846) Abcam (ab178847)	Abcam (ab105593)	Yes	Yes	Yes
CNPase	Oligodendrocytes	Not available	Millipore (MAB326) CST (5664)	Requires custom synthesis	Yes	Yes	Yes
MAP2	Neurons (dendrites)	Not available	PhosphoSolutions (1099-MAP2)	Requires characterization & custom synthesis	Yes	Yes	Yes
GFAP	Astrocytes	F211M (human)	Included in kit	Included in kit	Yes	Yes	No
Tau (total)	Neurons (axons)	F218D (human) F228E (mouse)	Included in kit	Included in kit	No[a]	Yes[a]	No

[a]For analysis of total Tau, monkey samples were tested using the human kit (F218D) and rat samples were tested using the mouse kit (F228E).

Chromatography (CEX column) and then dialyzed with the final formulation. Vector genome titers were quantified using SYBR green-based qPCR with primers against the ITRs. The titer of AAV-PHP.b-CBh-SMN1 and proprietary AAV9 vector was determined to be 5×10^{13} vg/mL and 4.35×10^{13} vg/mL, respectively.

Histopathology

Representative DRG samples with their respective nerve roots (dorsal, ventral, and spinal nerve roots) were collected bilaterally from the cervical, thoracic, and lumbar regions of the rats (C3, T6, and L4) and monkeys (C1, C4, T3, L3, and L5). Nerve roots were evaluated instead of the standard recommended nerves (sciatic, tibial, radial, median, sural, saphenous, peroneal)[62] because neuronal degeneration is the primary toxicity associated with AAV vectors, while any effect on peripheral nerves is secondary.[22] Cross sections of the cervical, thoracic, and lumbar regions of the spinal cord were also evaluated in the rats (C3, T6, and L4) and monkeys (C1, C4, T3, L3, and L5). Samples were fixed in 10% neutral buffered formalin, embedded in paraffin, sectioned longitudinally at 5 μm thickness, and stained with H&E within 72 h of collection, according to standard protocols. Slides were evaluated and reviewed by board-certified veterinary pathologists. Images were scanned using a Leica Aperio AT2 digital whole slide scanner and acquired using ImageScope viewing software (Leica Biosystems, Vista, CA). Microscopic findings were graded on the following scale: 1 = minimal, 2 = mild, 3 = moderate, 4 = marked, and 5 = severe, where the reported severity grade per animal was based on the most severe lesion observed.

Identification of cell-specific candidate biomarkers

Proteins commonly used to evaluate cell- and structure-specific neurotoxicity via immunohistochemistry were identified as candidate biomarkers for DRG toxicity. This included the following: (1) UCH-L1 for neurons,[63] (2) Tau and NF-L for axons,[64,65] (3) microtubule-associated protein 2 (MAP2) for neuron dendrites,[66] (4) GFAP for astrocytes,[67] (5) 2′,3′-cyclic-nucleotide 3′-phosphodiesterase (CNPase) for oligodendrocytes,[68] and (6) ionized calcium binding adaptor molecule 1 (IBA1) for microglia (CNS) and macrophages (PNS).[67] The expression profile of each candidate was then examined using internal transcriptomic and proteomic tissue atlases. With the exception of IBA1, each candidate was highly enriched within nervous system tissues (e.g., cerebral cortex, spinal cord, DRGs) at both the mRNA and protein levels. Although IBA1 is expressed by all macrophages throughout the body, it remained a potential candidate as no microglia-specific markers have been identified to date. Preliminary data (internal unpublished data) indicated that serum NF-L was a particularly promising candidate, where increases were detected in cynomolgus monkeys exhibiting AAV-induced DRG toxicity.

To gauge the feasibility of developing ligand-binding assays for these biomarker candidates, the commercial availability of antibodies and recombinant protein standards was evaluated (Table 3). MSD R-PLEX kits, which include a capture and detection antibody pair along with a matched calibrator, are available for human UCH-L1 (F211O), NF-L (F217X), GFAP (F211M), and total Tau (F218D), while a mouse-specific R-PLEX kit for total Tau is also available (F228E). For IBA1, a pair of monoclonal antibodies (clone EPR16588, ab178846; clone EPR16589, ab178847) and a recombinant human protein (ab105593) are available from Abcam (Waltham, MA). Similarly, monoclonal antibodies against CNPase are available from EMD Millipore (clone 11-5B, MAB326) and Cell Signaling Technology (clone D83E10, 5664), while PhosphoSolutions offers a polyclonal antibody against MAP2 (1099-MAP2). Large quantities of high-quality recombinant proteins were not commercially available for either CNPase or MAP2, and thus calibrators for these candidates would require custom synthesis.

Capillary electrophoresis analysis of antibody cross-reactivity

To confirm cross-reactivity across species, each antibody discussed above was tested on brain lysate, DRG lysate, serum, and/or CSF using the ProteinSimple Wes capillary electrophoresis system (ProteinSimple, San Jose, CA). Brain and DRG samples from up to four donors per species were homogenized in Tissue Protein

Extraction Reagent (T-PER) supplemented with HALT protease inhibitor and benzonase endonuclease using a Tissue Lyser Mixer Mill Grinder (Qiagen), while serum and CSF were directly diluted in supplemented T-PER. Samples were centrifuged at 10,000 × *g* for 5 min and total protein in the supernatant was measured using the bicinchoninic acid (BCA) assay (Sigma). Primary antibodies were detected using a secondary antibody conjugated to horseradish peroxidase. Up to three separate plates were run for each antibody, with samples grouped as follows: (1) human brain, monkey brain, monkey DRGs, (2) rat brain, rat DRGs, mouse brain, and (3) monkey serum/CSF, rat serum/CSF. Chemiluminescence signals were analyzed with Compass software (ProteinSimple), where image contrast was adjusted separately for each antibody to visualize the presence versus absence of the target peak(s).

MSD assay development

A duplex MSD assay was developed by combining R-PLEX kits for NF-L (F217X) and UCH-L1 (F211O) with the U-PLEX 2-Assay Development Pack (K15227N). As per the manufacturer's protocol, biotinylated NF-L and UCH-L1 capture antibodies were incubated with U-PLEX linker #1 and #10, respectively, followed by quenching with Stop Solution. Linked capture antibodies were further diluted 10-fold in Stop Solution prior to coating the U-PLEX plate; detection antibodies were diluted 100-fold in Diluent 3. Using Diluent 43, rat plasma and serum were diluted 4-fold, while rat CSF and cynomolgus monkey serum, plasma, and CSF were diluted 6-fold. Recombinant NF-L and UCH-L1 calibrators were diluted to 25,000 and 400,000 pg/mL, respectively, in Diluent 43 to yield the top standard. An 8-point curve (including a blank) was then prepared by serial 4-fold dilutions of the top standard. The assay consisted of the following steps: (1) 50 µL/well 1x duplex coating solution, (2) 50 µL/well diluted samples or standards, and (3) 50 µL/well 1x detection antibody mix. At each step, the plate was incubated with shaking (700 rpm) for 1 h at room temperature, followed by 3 × 200 µL washes with 1x MSD Wash Buffer. Immediately following the final wash, 150 µL MSD GOLD Read Buffer A was added to each well and the plate was read on a MESO SECTOR S 600.

A "fit-for-purpose" assay validation involving the following tests was performed for rat plasma: (1) intra-assay precision and accuracy, (2) inter-assay precision and accuracy, (3) freeze-thaw stability, and (4) dilution linearity. Bridging validations were performed for additional biological matrices including rat CSF and serum, as well as cynomolgus monkey CSF, serum, and plasma. Only intra-assay precision/accuracy and dilution linearity were evaluated in bridging validations. Validation criteria are listed in Table S3. QC samples were prepared by spiking high, mid, and low levels of NF-L and UCH-L1 calibrators into the biological matrix of interest, while detection limits were determined by diluting calibrators directly in Diluent 43. A singleplex version of the MSD assay was also developed for NF-L using the same reagents and kits described above, where spot 1 was linked to the NF-L capture antibody and spot 10 was left empty. To ensure comparability against the fully validated duplex version, a plate was run with half the wells in duplex format and the other half in singleplex format. In this side-by-side comparison, the singleplex versus duplex values were compared for each NF-L standard on the curve, along with high, mid, and low levels of NF-L calibrator spiked into rat plasma and monkey serum.

During validation, samples and standards were run in 3 to 6 replicates, while study samples were analyzed in duplicate. For each plate, the MSD software sets the lower LOD as 2.5 SDs above the blank. Any samples falling below the LOD were reported as the LOD value for that plate.

Quanterix analysis of biomarkers

NF-L in rat plasma, monkey serum, and monkey CSF was quantified by Quanterix Accelerator Lab Services (Billerica, MA) using the Simoa HD-X Neurology 4-Plex Panel B (N4PB) assay. Of the four biomarkers included in this panel, only NF-L is reported here; the assays for GFAP, UCH-L1, and total Tau exhibit poor cross-reactivity against rat and/or monkey samples and thus these data were not analyzed. Rat plasma and monkey CSF were diluted 40-fold in sample diluent, while monkey serum was diluted either 4- or 8-fold.

Statistical analysis

Statistical analysis was performed in GraphPad Prism 9.0.0, where p values ≤ 0.05 were considered significant. For biomarker data in rats, significance was evaluated through either a Kruskal-Wallis test followed by Dunn's multiple comparison test (dose, severity) or Welch's t test (presence versus absence of DRG toxicity). For biomarker data in monkeys, significance was evaluated through either one-way ANOVA analysis followed by Dunnett's multiple comparison test (dose, severity) or t test (presence versus absence of DRG toxicity). For naive biomarker levels, sex- and matrix-related differences were evaluated through two-way ANOVA analysis followed by Sidak's multiple comparisons test. Coefficient of determination (R^2) values were determined through linear regression analysis.

SUPPLEMENTAL INFORMATION

Supplemental information can be found online at https://doi.org/10.1016/j.omtm.2022.03.017.

ACKNOWLEDGMENTS

The authors thank Joseph T. Brady and Jon C. Cook for their support throughout the project and review of the manuscript; Thomas A. Lanz, Chang-Ning Liu, and Laurence O. Whiteley for critical review of the manuscript; June Liu for her help with study conduct and protocols; Colleen M. Doshna, Lauren Martin, and Kimberly S. Ebersole for performing QC of the study data; Ryan Criswell, Taylor Hulten, Linda M. Hutter, James A. Stejskal, and Gretchen L. Volberg for their help with sample procurement. The study was funded by Pfizer Worldwide Research, Development and Medical, Drug Safety Research and Development.

AUTHOR CONTRIBUTIONS

K.A.F., I.D.P., C.J.S., H.H.W., and M.P.S. conceptualized the studies; I.D.P. performed histopathology assessment; K.A.F. conducted method development and sample analysis; K.A.F. and M.P.S. analyzed and interpreted data; K.A.F. and M.P.S. drafted the manuscript; K.A.F., I.D.P., C.J.S., R.C.K., H.H.W., V.S.V., S.K.R., and M.P.S. critically reviewed and revised the manuscript.

DECLARATION OF INTERESTS

K.A.F., R.C.K., C.J.S., H.H.W., V.S.V., S.K.R., and M.P.S. are employees of Pfizer Inc.; I.D.P. is now an employee of Biogen. All authors are/were employees of Pfizer Inc. at the time of their contribution to the manuscript.

REFERENCES

1. Balakrishnan, B., and Jayandharan, G.R. (2014). Basic biology of adeno-associated virus (AAV) vectors used in gene therapy. Curr. Gene Ther. *14*, 86–100.
2. Naso, M.F., Tomkowicz, B., Perry, W.L., 3rd, and Strohl, W.R. (2017). Adeno-associated virus (AAV) as a vector for gene therapy. Biodrugs *31*, 317–334.
3. Colella, P., Ronzitti, G., and Mingozzi, F. (2018). Emerging issues in AAV-mediated in vivo gene therapy. Mol. Ther. Methods Clin. Dev. *8*, 87–104.
4. Li, C., and Samulski, R.J. (2020). Engineering adeno-associated virus vectors for gene therapy. Nat. Rev. Genet. *21*, 255–272.
5. Bolt, M.W., Brady, J.T., Whiteley, L.O., and Khan, K.N. (2021). Development challenges associated with rAAV-based gene therapies. J. Toxicol. Sci. *46*, 57–68.
6. Ronzitti, G., Gross, D.A., and Mingozzi, F. (2020). Human immune responses to adeno-associated virus (AAV) vectors. Front. Immunol. *11*, 670.
7. Kuranda, K., Jean-Alphonse, P., Leborgne, C., Hardet, R., Collaud, F., Marmier, S., Costa Verdera, H., Ronzitti, G., Veron, P., and Mingozzi, F. (2018). Exposure to wild-type AAV drives distinct capsid immunity profiles in humans. J. Clin. Invest. *128*, 5267–5279.
8. Ertl, H.C.J., and High, K.A. (2017). Impact of AAV capsid-specific T-cell responses on design and outcome of clinical gene transfer trials with recombinant adeno-associated viral vectors: an evolving controversy. Hum. Gene Ther. *28*, 328–337.
9. Mendell, J.R., Sahenk, Z., Lehman, K., Nease, C., Lowes, L.P., Miller, N.F., Iammarino, M.A., Alfano, L.N., Nicholl, A., Al-Zaidy, S., et al. (2020). Assessment of systemic delivery of rAAVrh74.MHCK7.micro-dystrophin in children with duchenne muscular dystrophy: a nonrandomized controlled trial. JAMA Neurol. *77*, 1122–1131.
10. Meliani, A., Boisgerault, F., Hardet, R., Marmier, S., Collaud, F., Ronzitti, G., Leborgne, C., Costa Verdera, H., Simon Sola, M., Charles, S., et al. (2018). Antigen-selective modulation of AAV immunogenicity with tolerogenic rapamycin nanoparticles enables successful vector re-administration. Nat. Commun. *9*, 4098.
11. Stone, D., Kenkel, E.J., Loprieno, M.A., Tanaka, M., De Silva Feelixge, H.S., Kumar, A.J., Stensland, L., Obenza, W.M., Wangari, S., Ahrens, C.Y., et al. (2021). Gene transfer in adeno-associated virus seropositive rhesus macaques following rapamycin treatment and subcutaneous delivery of AAV6, but not retargeted AAV6 vectors. Hum. Gene Ther. *32*, 96–112.
12. Palazzi, X., Pardo, I.D., Sirivelu, M.P., Newman, L., Kumpf, S.W., Qian, J., Franks, T., Lopes, S., Liu, J., Monarski, L., et al. (2022). Biodistribution and tolerability of AAV-PHP.B-CBh-SMN1 in wistar han rats and cynomolgus macaques reveal different toxicologic profiles. Hum. Gene Ther. *33*, 175–187.
13. Hinderer, C., Katz, N., Buza, E.L., Dyer, C., Goode, T., Bell, P., Richman, L.K., and Wilson, J.M. (2018). Severe toxicity in nonhuman primates and piglets following high-dose intravenous administration of an adeno-associated virus vector expressing human SMN. Hum. Gene Ther. *29*, 285–298.
14. Feldman, A.G., Parsons, J.A., Dutmer, C.M., Veerapandiyan, A., Hafberg, E., Maloney, N., and Mack, C.L. (2020). Subacute liver failure following gene replacement therapy for spinal muscular atrophy type 1. J. Pediatr. *225*, 252–258.e1.
15. Donsante, A., Miller, D.G., Li, Y., Vogler, C., Brunt, E.M., Russell, D.W., and Sands, M.S. (2007). AAV vector integration sites in mouse hepatocellular carcinoma. Science *317*, 477.
16. Chandler, R.J., LaFave, M.C., Varshney, G.K., Trivedi, N.S., Carrillo-Carrasco, N., Senac, J.S., Wu, W., Hoffmann, V., Elkahloun, A.G., Burgess, S.M., et al. (2015). Vector design influences hepatic genotoxicity after adeno-associated virus gene therapy. J. Clin. Invest. *125*, 870–880.
17. Hordeaux, J., Buza, E.L., Jeffrey, B., Song, C., Jahan, T., Yuan, Y., Zhu, Y., Bell, P., Li, M., Chichester, J.A., et al. (2020). MicroRNA-mediated inhibition of transgene expression reduces dorsal root ganglion toxicity by AAV vectors in primates. Sci. Transl. Med. *12*, eaba9188.
18. Hordeaux, J., Hinderer, C., Goode, T., Katz, N., Buza, E.L., Bell, P., Calcedo, R., Richman, L.K., and Wilson, J.M. (2018). Toxicology study of intra-cisterna magna adeno-associated virus 9 expressing human alpha-L-iduronidase in rhesus macaques. Mol. Ther. Methods Clin. Dev. *10*, 79–88.
19. Hordeaux, J., Hinderer, C., Goode, T., Buza, E.L., Bell, P., Calcedo, R., Richman, L.K., and Wilson, J.M. (2018). Toxicology study of intra-cisterna magna adeno-associated virus 9 expressing iduronate-2-sulfatase in rhesus macaques. Mol. Ther. Methods Clin. Dev. *10*, 68–78.
20. Hordeaux, J., Hinderer, C., Buza, E.L., Louboutin, J.P., Jahan, T., Bell, P., Chichester, J.A., Tarantal, A.F., and Wilson, J.M. (2019). Safe and sustained expression of human iduronidase after intrathecal administration of adeno-associated virus serotype 9 in infant rhesus monkeys. Hum. Gene Ther. *30*, 957–966.
21. Van Alstyne, M., Tattoli, I., Delestree, N., Recinos, Y., Workman, E., Shihabuddin, L.S., Zhang, C., Mentis, G.Z., and Pellizzoni, L. (2021). Gain of toxic function by long-term AAV9-mediated SMN overexpression in the sensorimotor circuit. Nat. Neurosci. *24*, 930–940.
22. Hordeaux, J., Buza, E.L., Dyer, C., Goode, T., Mitchell, T.W., Richman, L., Denton, N., Hinderer, C., Katz, N., Schmid, R., et al. (2020). Adeno-associated virus-induced dorsal root ganglion pathology. Hum. Gene Ther. *31*, 808–818.
23. Mueller, C., Berry, J.D., McKenna-Yasek, D.M., Gernoux, G., Owegi, M.A., Pothier, L.M., Douthwright, C.L., Gelevski, D., Luppino, S.D., Blackwood, M., et al. (2020). SOD1 suppression with adeno-associated virus and MicroRNA in familial ALS. N. Engl. J. Med. *383*, 151–158.
24. Mason, M.R., Ehlert, E.M., Eggers, R., Pool, C.W., Hermening, S., Huseinovic, A., Timmermans, E., Blits, B., and Verhaagen, J. (2010). Comparison of AAV serotypes for gene delivery to dorsal root ganglion neurons. Mol. Ther. *18*, 715–724.
25. Toscano, M.G., Romero, Z., Munoz, P., Cobo, M., Benabdellah, K., and Martin, F. (2011). Physiological and tissue-specific vectors for treatment of inherited diseases. Gene Ther. *18*, 117–127.
26. Kelly, E.J., and Russell, S.J. (2009). MicroRNAs and the regulation of vector tropism. Mol. Ther. *17*, 409–416.
27. Aldrich, B.T., Frakes, E.P., Kasuya, J., Hammond, D.L., and Kitamoto, T. (2009). Changes in expression of sensory organ-specific microRNAs in rat dorsal root ganglia in association with mechanical hypersensitivity induced by spinal nerve ligation. Neuroscience *164*, 711–723.
28. Pardo, I.D., Weber, K., Cramer, S., Krinke, G.J., Butt, M.T., Sharma, A.K., and Bolon, B. (2020). Atlas of normal microanatomy, procedural and processing artifacts, common background findings, and neurotoxic lesions in the peripheral nervous system of laboratory animals. Toxicol. Pathol. *48*, 105–131.
29. Boehnke, S.E., Robertson, E.L., Armitage-Brown, B., Wither, R.G., Lyra, E.S.N.M., Winterborn, A., Levy, R., Cook, D.J., De Felice, F.G., and Munoz, D.P. (2020). The effect of lumbar puncture on the neurodegeneration biomarker neurofilament light in macaque monkeys. Alzheimers Dement. (Amst). *12*, e12069.
30. Bergman, J., Dring, A., Zetterberg, H., Blennow, K., Norgren, N., Gilthorpe, J., Bergenheim, T., and Svenningsson, A. (2016). Neurofilament light in CSF and serum is a sensitive marker for axonal white matter injury in MS. Neurol. Neuroimmunol. Neuroinflamm. *3*, e271.
31. Kim, S.H., Choi, M.K., Park, N.Y., Hyun, J.W., Lee, M.Y., Kim, H.J., Jung, S.K., and Cha, Y. (2020). Serum neurofilament light chain levels as a biomarker of neuroaxonal injury and severity of oxaliplatin-induced peripheral neuropathy. Sci. Rep. *10*, 7995.
32. Yuan, A., Rao, M.V., Veeranna, and Nixon, R.A. (2017). Neurofilaments and neurofilament proteins in health and disease. Cold Spring Harb. Perspect. Biol. *9*, a018309.

33. Soylu-Kucharz, R., Sandelius, A., Sjogren, M., Blennow, K., Wild, E.J., Zetterberg, H., and Bjorkqvist, M. (2017). Neurofilament light protein in CSF and blood is associated with neurodegeneration and disease severity in Huntington's disease R6/2 mice. Sci. Rep. *7*, 14114.

34. Le, N.D., Muri, L., Grandgirard, D., Kuhle, J., Leppert, D., and Leib, S.L. (2020). Evaluation of neurofilament light chain in the cerebrospinal fluid and blood as a biomarker for neuronal damage in experimental pneumococcal meningitis. J. Neuroinflammation *17*, 293.

35. Vlasakova, K., Qin, C., Tsuchiya, T., Dey, M., Zhou, Y., and Glaab, W. (2019). Performance of neurofilament light in rat as a translational biomarker of central and peripheral nervous system toxicity (1484a). Toxicologist *168*, 116.

36. Sano, T., Masuda, Y., Yasuno, H., Shinozawa, T., Watanabe, T., and Kakehi, M. (2021). Blood neurofilament light chain as a potential biomarker for central and peripheral nervous toxicity in rats. Toxicol. Sci. *185*, 10–18.

37. Korley, F.K., Yue, J.K., Wilson, D.H., Hrusovsky, K., Diaz-Arrastia, R., Ferguson, A.R., Yuh, E.L., Mukherjee, P., Wang, K.K.W., Valadka, A.B., et al. (2018). Performance evaluation of a multiplex assay for simultaneous detection of four clinically relevant traumatic brain injury biomarkers. J. Neurotrauma *36*, 182–187.

38. Zetterberg, H., Hietala, M.A., Jonsson, M., Andreasen, N., Styrud, E., Karlsson, I., Edman, A., Popa, C., Rasulzada, A., Wahlund, L.O., et al. (2006). Neurochemical aftermath of amateur boxing. Arch. Neurol. *63*, 1277–1280.

39. Shahim, P., Zetterberg, H., Tegner, Y., and Blennow, K. (2017). Serum neurofilament light as a biomarker for mild traumatic brain injury in contact sports. Neurology *88*, 1788–1794.

40. Hendricks, R., Baker, D., Brumm, J., Davancaze, T., Harp, C., Herman, A., Budingen, H.V., Townsend, M., and Fischer, S.K. (2019). Establishment of neurofilament light chain Simoa assay in cerebrospinal fluid and blood. Bioanalysis *11*, 1405–1418.

41. Gaiottino, J., Norgren, N., Dobson, R., Topping, J., Nissim, A., Malaspina, A., Bestwick, J.P., Monsch, A.U., Regeniter, A., Lindberg, R.L., et al. (2013). Increased neurofilament light chain blood levels in neurodegenerative neurological diseases. PLoS One *8*, e75091.

42. Norgren, N., Rosengren, L., and Stigbrand, T. (2003). Elevated neurofilament levels in neurological diseases. Brain Res. *987*, 25–31.

43. Alves, C.R.R., Petrillo, M., Spellman, R., Garner, R., Zhang, R., Kiefer, M., Simeone, S., Sohn, J., Eichelberger, E.J., Rodrigues, E., et al. (2021). Implications of circulating neurofilamentsfor spinal muscular atrophytreatment early in life: a case series. Mol. Ther. Methods Clin. Dev. *23*, 524–538.

44. Haberberger, R.V., Barry, C., Dominguez, N., and Matusica, D. (2019). Human dorsal root ganglia. Front. Cell Neurosci. *13*, 271.

45. Esposito, M.F., Malayil, R., Hanes, M., and Deer, T. (2019). Unique characteristics of the dorsal root ganglion as a target for neuromodulation. Pain Med. *20* (*Suppl 1*), S23–S30.

46. Godel, T., Pham, M., Heiland, S., Bendszus, M., and Baumer, P. (2016). Human dorsal-root-ganglion perfusion measured in-vivo by MRI. Neuroimage *141*, 81–87.

47. Kiernan, J.A. (1996). Vascular permeability in the peripheral autonomic and somatic nervous systems: controversial aspects and comparisons with the blood-brain barrier. Microsc. Res. Tech. *35*, 122–136.

48. Liu, M.C., Akinyi, L., Scharf, D., Mo, J., Larner, S.F., Muller, U., Oli, M.W., Zheng, W., Kobeissy, F., Papa, L., et al. (2010). Ubiquitin C-terminal hydrolase-L1 as a biomarker for ischemic and traumatic brain injury in rats. Eur. J. Neurosci. *31*, 722–732.

49. Papa, L., Akinyi, L., Liu, M.C., Pineda, J.A., Tepas, J.J., 3rd, Oli, M.W., Zheng, W., Robinson, G., Robicsek, S.A., Gabrielli, A., et al. (2010). Ubiquitin C-terminal hydrolase is a novel biomarker in humans for severe traumatic brain injury. Crit. Care Med. *38*, 138–144.

50. Kawata, K., Liu, C.Y., Merkel, S.F., Ramirez, S.H., Tierney, R.T., and Langford, D. (2016). Blood biomarkers for brain injury: what are we measuring? Neurosci. Biobehav. Rev. *68*, 460–473.

51. Sundaramoorthy, V., Green, D., Locke, K., O'Brien, C.M., Dearnley, M., and Bingham, J. (2020). Novel role of SARM1 mediated axonal degeneration in the pathogenesis of rabies. PLoS Pathog. *16*, e1008343.

52. Schartz, N.D., Herr, S.A., Madsen, L., Butts, S.J., Torres, C., Mendez, L.B., and Brewster, A.L. (2016). Spatiotemporal profile of Map2 and microglial changes in the hippocampal CA1 region following pilocarpine-induced status epilepticus. Sci. Rep. *6*, 24988.

53. Li, G.L., Farooque, M., Lewen, A., Lennmyr, F., Holtz, A., and Olsson, Y. (2000). MAP2 and neurogranin as markers for dendritic lesions in CNS injury. An immunohistochemical study in the rat. APMIS *108*, 98–106.

54. Park, D., Joo, S.S., Lee, H.J., Choi, K.C., Kim, S.U., and Kim, Y.B. (2012). Microtubule-associated protein 2, an early blood marker of ischemic brain injury. J. Neurosci. Res. *90*, 461–467.

55. Daftary, S., Yon, J.M., Choi, E.K., Kim, Y.B., Bice, C., Kulikova, A., Park, J., and Sherwood Brown, E. (2017). Microtubule associated protein 2 in bipolar depression: impact of pregnenolone. J. Affect Disord. *218*, 49–52.

56. Bridel, C., Verberk, I.M.W., Heijst, J.J.A., Killestein, J., and Teunissen, C.E. (2021). Variations in consecutive serum neurofilament light levels in healthy controls and multiple sclerosis patients. Mult. Scler. Relat. Disord. *47*, 102666.

57. Khalil, M., Pirpamer, L., Hofer, E., Voortman, M.M., Barro, C., Leppert, D., Benkert, P., Ropele, S., Enzinger, C., Fazekas, F., et al. (2020). Serum neurofilament light levels in normal aging and their association with morphologic brain changes. Nat. Commun. *11*, 812.

58. Huehnchen, P., Schinke, C., Bangemann, N., Dordevic, A.D., Kern, J., Maierhof, S.K., Hew, L., Nolte, L., Kortvelyessy, P., Gopfert, J.C., et al. (2022). Neurofilament Proteins as Potential Biomarker in Chemotherapy-Induced Polyneuropathy (JCI Insight).

59. U.S. FDA (2021). Biomarker qualification submissions. https://cacmap.fda.gov/drugs/biomarker-qualification-program/biomarker-qualification-submissions.

60. Leptak, C.L., and Kozauer, N. (2020). Letter of intent - determination letter (DDTBMQ000101). https://www.fda.gov/media/140339/download.

61. Bridel, C., Leurs, C.E., van Lierop, Z., van Kempen, Z.L.E., Dekker, I., Twaalfhoven, H.A.M., Moraal, B., Barkhof, F., Uitdehaag, B.M.J., Killestein, J., et al. (2021). Serum neurofilament light association with progression in natalizumab-treated patients with relapsing-remitting multiple sclerosis. Neurology *97*, e1898–e1905.

62. Bolon, B., Krinke, G., Butt, M.T., Rao, D.B., Pardo, I.D., Jortner, B.S., Garman, R.H., Jensen, K., Andrews-Jones, L., Morrison, J.P., et al. (2018). STP position paper: recommended best practices for sampling, processing, and analysis of the peripheral nervous system (nerves and somatic and autonomic ganglia) during nonclinical toxicity studies. Toxicol. Pathol. *46*, 372–402.

63. Wilson, P.O., Barber, P.C., Hamid, Q.A., Power, B.F., Dhillon, A.P., Rode, J., Day, I.N., Thompson, R.J., and Polak, J.M. (1988). The immunolocalization of protein gene product 9.5 using rabbit polyclonal and mouse monoclonal antibodies. Br. J. Exp. Pathol. *69*, 91–104.

64. Kanaan, N.M., and Grabinski, T. (2021). Neuronal and glial distribution of Tau protein in the adult rat and monkey. Front. Mol. Neurosci. *14*, 607303.

65. Mages, B., Aleithe, S., Altmann, S., Blietz, A., Nitzsche, B., Barthel, H., Horn, A.K.E., Hobusch, C., Hartig, W., Krueger, M., et al. (2018). Impaired neurofilament integrity and neuronal morphology in different models of focal cerebral ischemia and human stroke tissue. Front. Cell Neurosci. *12*, 161.

66. Gumy, L.F., Katrukha, E.A., Grigoriev, I., Jaarsma, D., Kapitein, L.C., Akhmanova, A., and Hoogenraad, C.C. (2017). MAP2 defines a pre-axonal filtering zone to regulate KIF1- versus KIF5-dependent cargo transport in sensory neurons. Neuron *94*, 347–362.e7.

67. Yun, S., Kim, W., Kang, M.S., Kim, T.H., Kim, Y., Ahn, J.O., Choi, J.H., Hwang, I.K., and Chung, J.Y. (2020). Neuropathological changes in dorsal root ganglia induced by pyridoxine in dogs. BMC Neurosci. *21*, 11.

68. Toma, J.S., McPhail, L.T., and Ramer, M.S. (2007). Differential RIP antigen (CNPase) expression in peripheral ensheathing glia. Brain Res. *1137*, 1–10.

OMTM, Volume *25*

Supplemental information

Circulating neurofilament light chain as a promising biomarker of AAV-induced dorsal root ganglia toxicity in nonclinical toxicology species

Kelly A. Fader, Ingrid D. Pardo, Ramesh C. Kovi, Christopher J. Somps, Helen Hong Wang, Vishal S. Vaidya, Shashi K. Ramaiah, and Madhu P. Sirivelu

SUPPLEMENTARY FIGURES

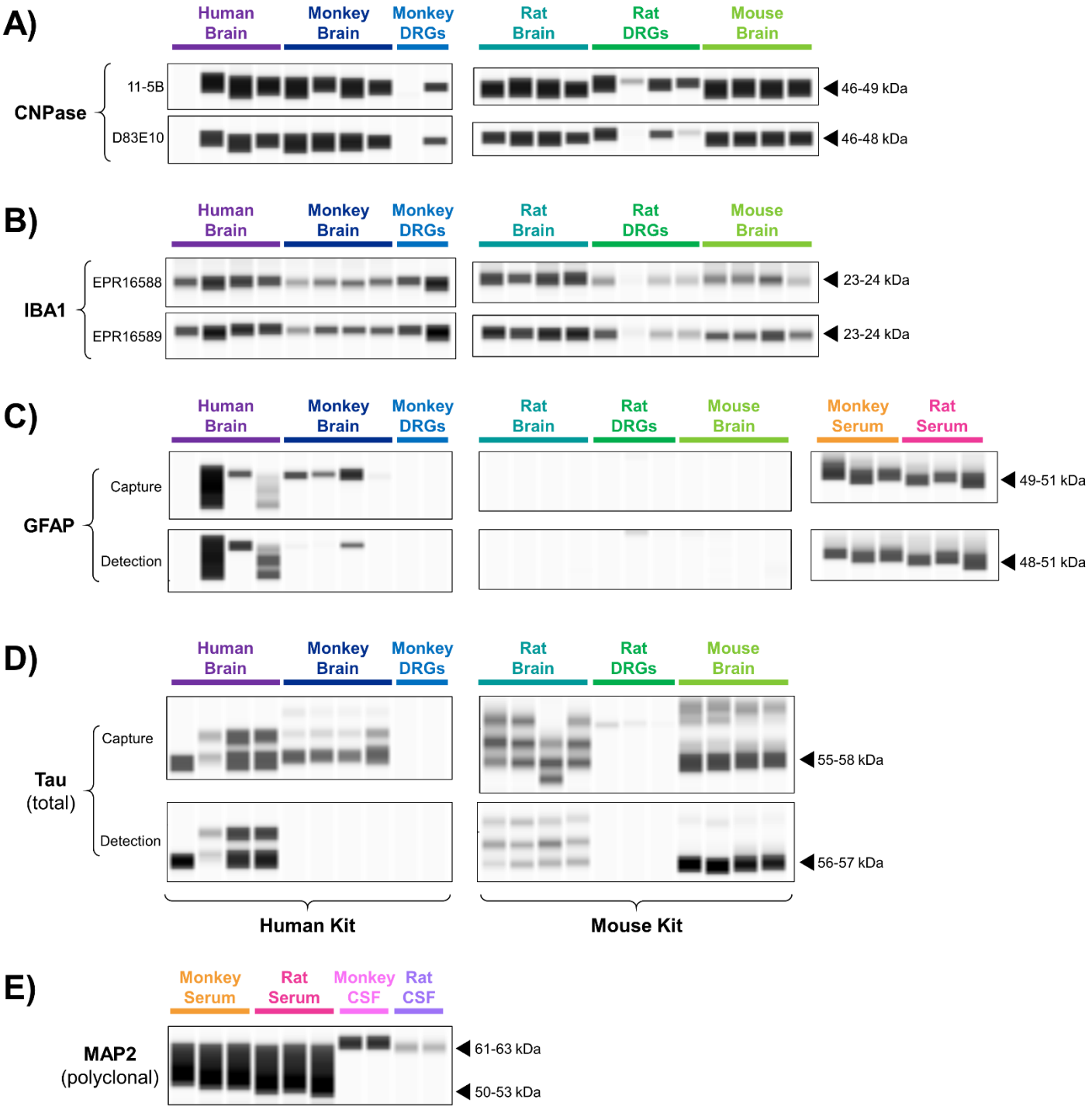

Supplementary Figure S1: Detection of candidate biomarkers in brain, dorsal root ganglia (DRG), and biofluids from human and nonclinical species. Wes capillary electrophoresis (ProteinSimple) was used to evaluate antibody cross-reactivity against brain homogenate (n=4) from human, cynomolgus monkey, Wistar Han rat, and CD1 mouse. Dissected DRGs (n=2-4), serum (n=3), and/or CSF (n=2) from monkey and rat were also assessed. A) CNPase antibody clones 11-5B and D83E10 were obtained from Millipore (MAB326) and Cell Signaling Technologies (5664), respectively. B) IBA1 antibody clones EPR16588 and ERP16589 were obtained from Abcam (ab178846 and ab178847, respectively). Meso Scale Discovery (MSD) R-PLEX kits were available for C) GFAP (human: F211M) and D) total Tau (human: F218D; mouse: F228E). E) The polyclonal antibody against MAP2 was obtained from PhosphoSolutions (1099-MAP2). Chemiluminescence signals were analyzed with Compass software (ProteinSimple), where image contrast was adjusted separately for each antibody to visualize the presence vs. absence of the target peak(s).

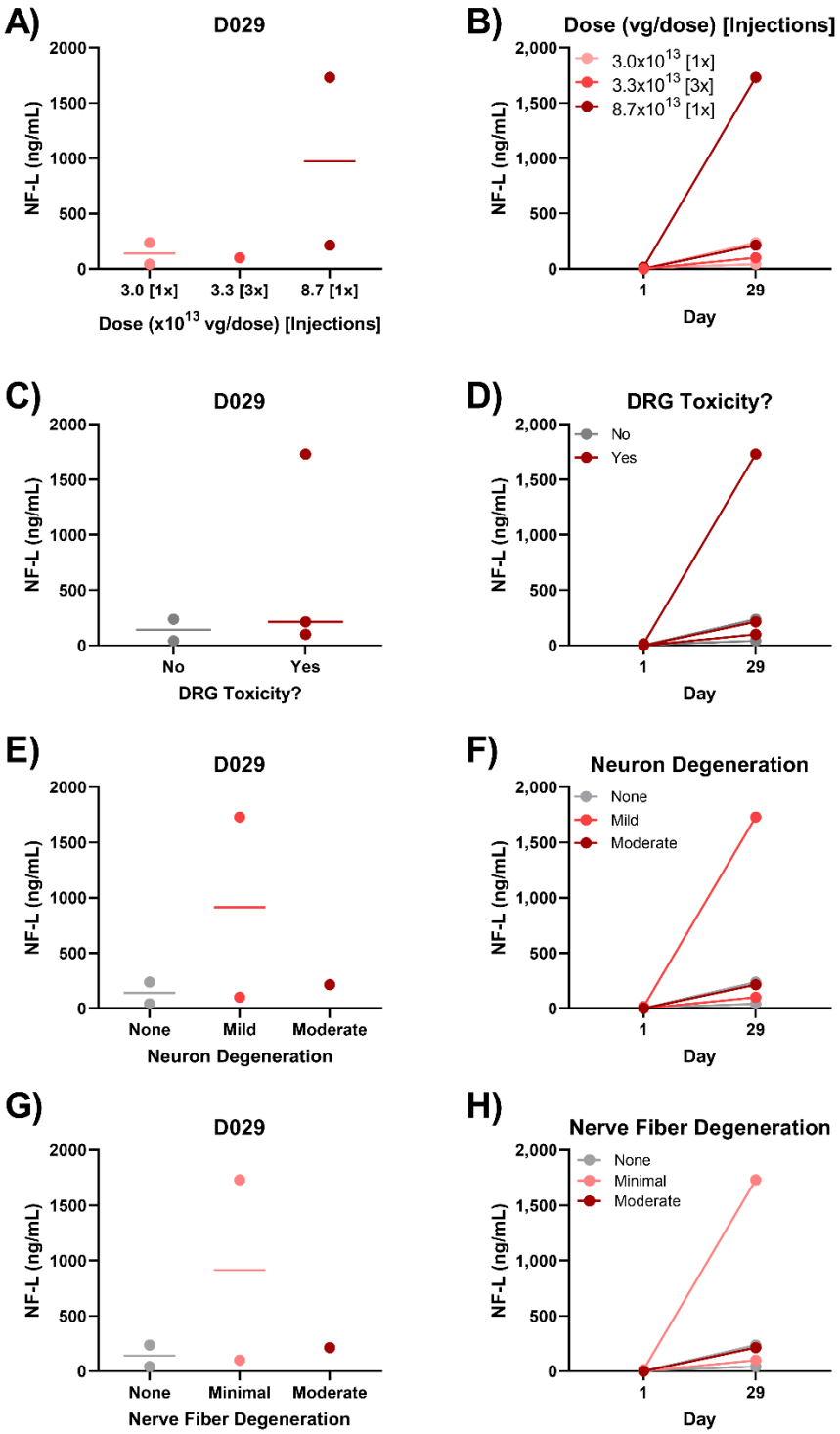

Supplementary Figure S2: NF-L in cerebrospinal fluid (CSF) from cynomolgus monkeys exhibiting AAV-induced dorsal root ganglia (DRG) toxicity. Male cynomolgus macaques (n=2 per group) were injected with $3.0x10^{13}$ [1x], $3.3x10^{13}$ [3x], or $8.7x10^{13}$ [1x] vg/dose AAV vector via intrathecal catheter. CSF was collected on Day 1 (pre-dose) and 29, while histologic DRG lesions were assessed on Day 29. NF-L in CSF was quantified using an in-house duplex Meso Scale Discovery (MSD) assay with a functional lower limit of quantification (LLOQ) of 144 pg/mL. NF-L was plotted against A) AAV dose, C) presence/absence of DRG toxicity (neuronal and/or nerve fiber degeneration), E) severity of DRG neuron degeneration/necrosis, and G) severity of DRG nerve fiber degeneration. Statistical significance ($p \leq 0.05$) was evaluated through one-way ANOVA analysis followed by Dunnett's multiple comparisons test (A, E, G) or t-test (C) performed in GraphPad Prism 9.0.0. NF-L for each animal has also been plotted by B) AAV dose, D) presence/absence of DRG toxicity (neuronal and/or nerve fiber degeneration), F) severity of DRG neuron degeneration/necrosis, and H) severity of DRG nerve fiber degeneration. Any values which fell below the limit of detection (LOD) were plotted as the functional LOD for that plate.

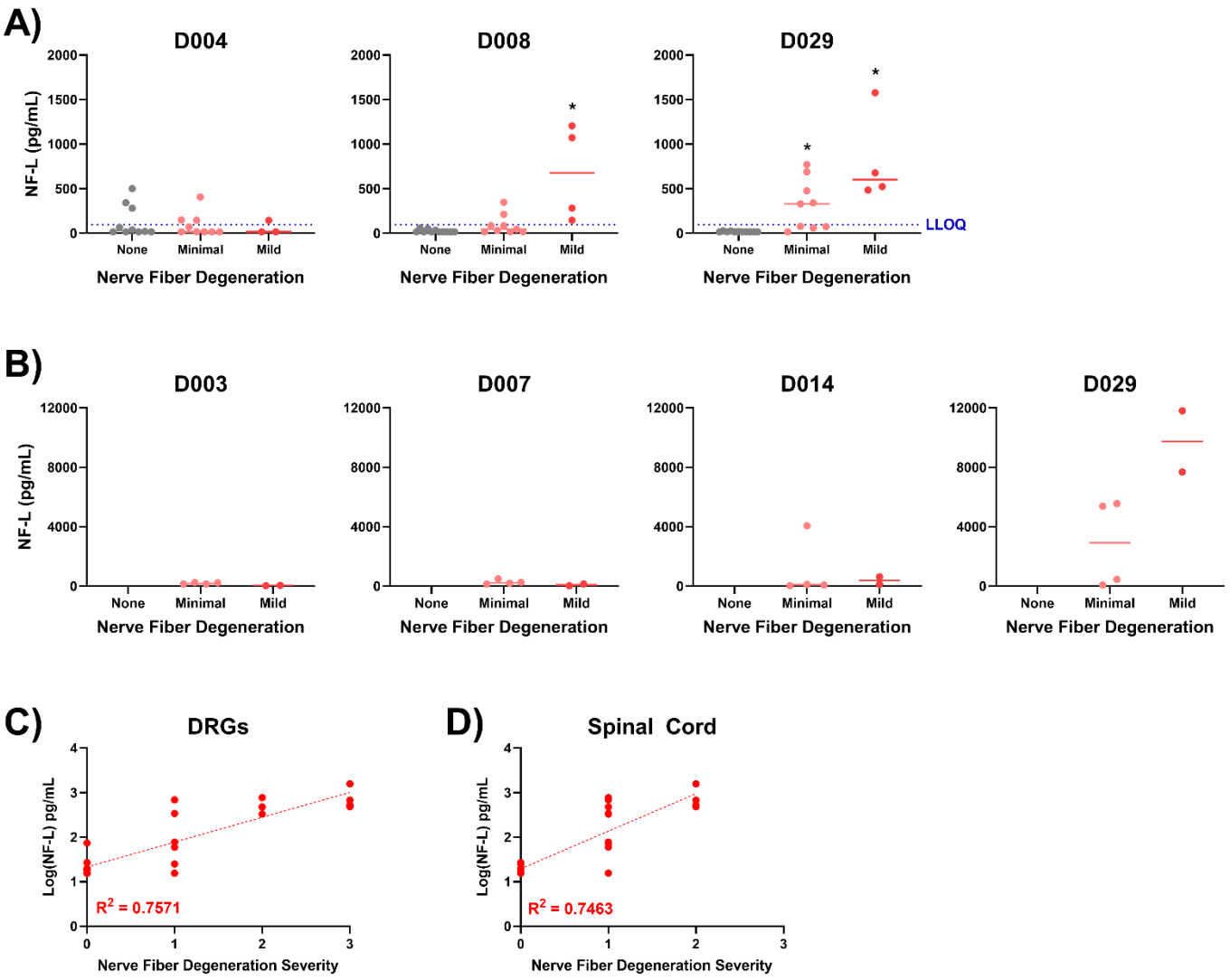

Supplementary Figure S3: Circulating NF-L is associated with the severity of nerve fiber degeneration in the spinal cord. A) Male Wistar Han rats (n=6) were intravenously injected with a bolus dose of 0, $2x10^{13}$, $5x10^{13}$, or $1x10^{14}$ vg/kg AAV vector. Plasma was collected 4, 8, and 29 days after injection, while histologic spinal cord lesions were assessed on Day 29. NF-L in plasma was quantified using an in-house duplex Meso Scale Discovery (MSD) assay with a functional lower limit of quantification (LLOQ) of 96 pg/mL. B) Male cynomolgus macaques (n=2) were injected with $3.0x10^{13}$ [1x], $3.3x10^{13}$ [3x], or $8.7x10^{13}$ [1x] vg/dose AAV vector via intrathecal catheter. Serum was collected 3, 7, 14, and 29 days after injection, while histologic spinal cord lesions were assessed on Day 29. NF-L in serum was quantified using an in-house duplex Meso Scale Discovery (MSD) assay with a functional LLOQ of 144 pg/mL. For each species, NF-L has been plotted against the severity of nerve fiber degeneration in the spinal cord. Statistical significance (* $p \leq 0.05$) was evaluated through a Kruskal-Wallis test followed by Dunn's multiple comparison test (A) or t-test (B) performed in GraphPad Prism 9.0.0. Any values which fell below the limit of detection (LOD) were plotted as the functional LOD for that plate. For rats, the correlation between log(NF-L) and nerve fiber degeneration is shown for C) dorsal root ganglia (DRGs) and D) the spinal cord, where the coefficient of determination (R^2) was determined through linear regression analysis. Severity grades of none, minimal, mild, and moderate have been assigned numerical scores of 0, 1, 2, and 3, respectively.

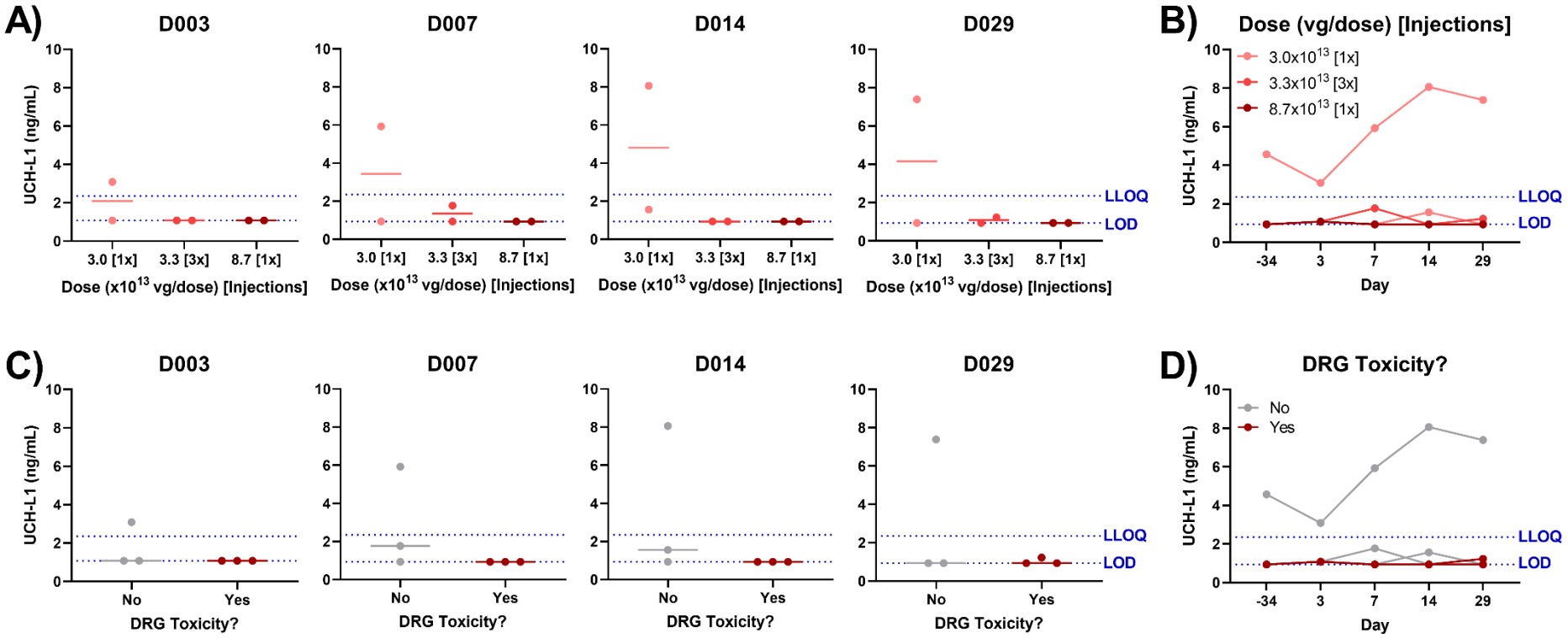

Supplementary Figure S4: UCH-L1 in serum from cynomolgus monkeys exhibiting AAV-induced dorsal root ganglia (DRG) toxicity. Male cynomolgus macaques (n=2 per group) were injected with $3.0x10^{13}$ [1x], $3.3x10^{13}$ [3x], or $8.7x10^{13}$ [1x] vg/dose AAV vector via intrathecal catheter. Serum was collected 3, 7, 14, and 29 days after injection, while histologic DRG lesions were assessed on Day 29. UCH-L1 in serum was quantified using an in-house duplex Meso Scale Discovery (MSD) assay. The blue dashed lines indicate the limit of detect (LOD) and lower limit of quantification (LLOQ) for the assay. UCH-L1 was plotted against A) AAV dose and C) presence/absence of DRG toxicity (neuronal and/or nerve fiber degeneration). Statistical significance ($p \leq 0.05$) was evaluated through one-way ANOVA analysis followed by Dunnett's multiple comparisons test (A) or t-test (C) performed in GraphPad Prism 9.0.0. The UCH-L1 profile for each animal was also plotted by B) AAV dose and D) presence/absence of DRG toxicity (neuronal and/or nerve fiber degeneration). Any values which fell below the limit of detection (LOD) were plotted as the functional LOD for that plate.

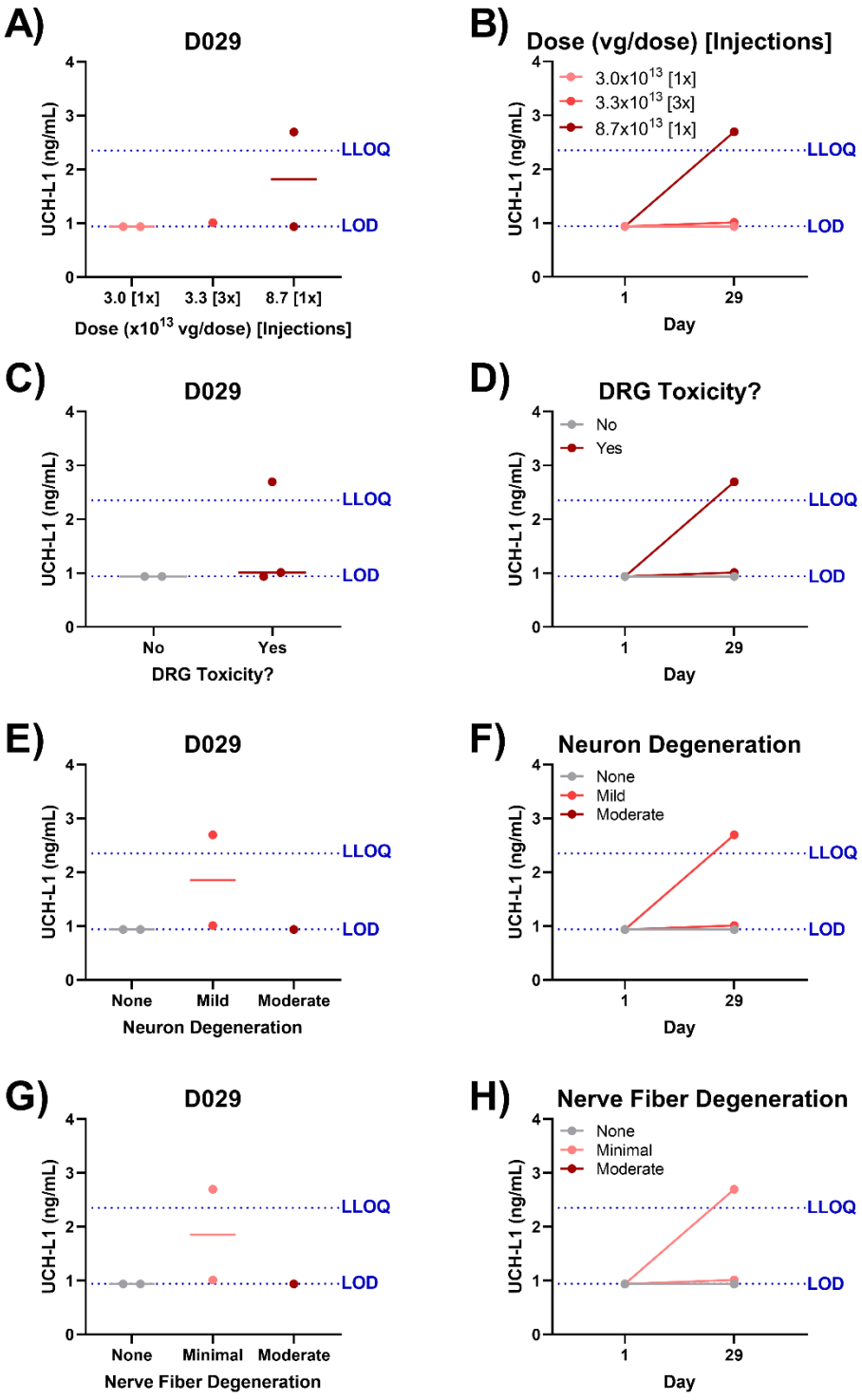

Supplementary Figure S5: UCH-L1 in cerebrospinal fluid (CSF) from cynomolgus monkeys exhibiting AAV-induced dorsal root ganglia (DRG) toxicity. Male cynomolgus macaques (n=2 per group) were injected with $3.0x10^{13}$ [1x], $3.3x10^{13}$ [3x], or $8.7x10^{13}$ [1x] vg/dose AAV vector via intrathecal catheter. CSF was collected on Day 1 (pre-dose) and 29, while histologic DRG lesions were assessed on Day 29. UCH-L1 in CSF was quantified using an in-house duplex Meso Scale Discovery (MSD) assay. The blue dashed lines indicate the limit of detect (LOD) and lower limit of quantification (LLOQ) for the assay. UCH-L1 was plotted against A) AAV dose, C) presence/absence of DRG toxicity (neuronal and/or nerve fiber degeneration), E) severity of DRG neuron degeneration/necrosis, and G) severity of DRG nerve fiber degeneration. Statistical significance ($p \leq 0.05$) was evaluated through one-way ANOVA analysis followed by Dunnett's multiple comparisons test (A, E, G) or t-test (C) performed in GraphPad Prism 9.0.0. The UCH-L1 profile for each animal was also plotted by B) AAV dose, D) presence/absence of DRG toxicity (neuronal and/or nerve fiber degeneration), F) severity of DRG neuron degeneration/necrosis, and H) severity of DRG nerve fiber degeneration. Any values which fell below the limit of detection (LOD) were plotted as the functional LOD for that plate.

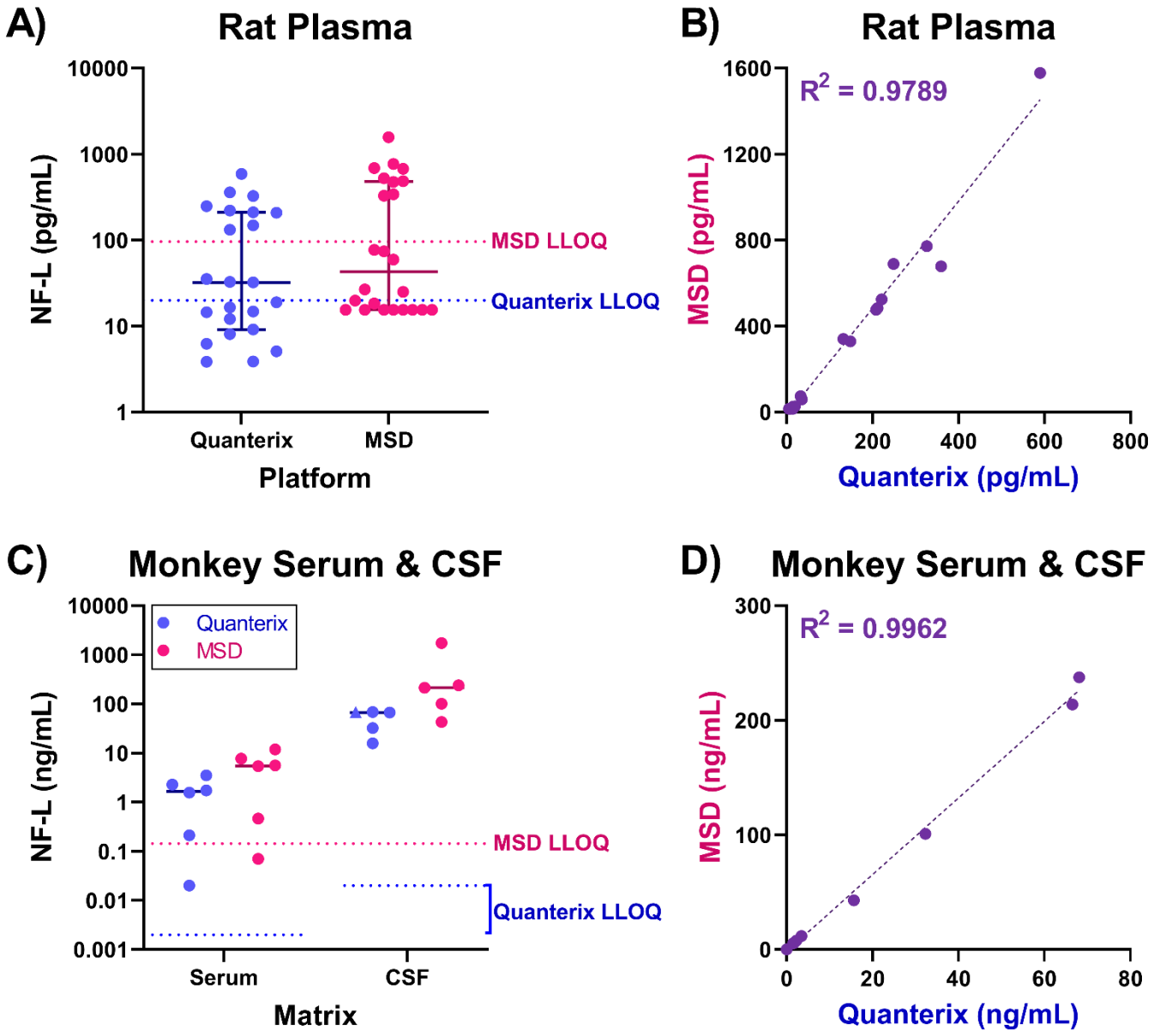

Supplementary Figure S6: NF-L values detected with an in-house Meso Scale Discovery (MSD) assay are highly correlated with Quanterix Simoa HD-X values. NF-L in A) rat plasma and C) cynomolgus monkey serum and cerebrospinal fluid (CSF) was evaluated using both the Quanterix Simoa Neurology 4-Plex Panel (blue) and an in-house duplex MSD assay (pink). The blue and pink dashed lines indicate the lower limit of quantification (LLOQ) for the Quanterix and MSD assays, respectively. The correlation between Quanterix and MSD values is shown for B) rats and D) monkeys, where the coefficient of determination (R^2) was determined through linear regression analysis. Any values which fell below the limit of detection (LOD) were plotted as the functional LOD for that assay. Note: The triangular data point (plot C) represents a sample which saturated the assay signal and thus has been plotted as the highest value obtained on the plate which did not saturate the signal. This sample was excluded from the correlation analysis (D).

SUPPLEMENTARY TABLES

Supplementary Table S1: Sensitivity of Meso Scale Discovery (MSD) duplex assay

Parameter	**NF-L** (pg/mL)	**UCH-L1** (pg/mL)
Limit of Detection (LOD)		
Analytical (average)	7.37	213
Functional (DF = 4)	29.50	851
Functional (DF=6)	44.24	1,277
Lower Limit of Quantification (LLOQ)		
Analytical	24	391
Functional (DF = 4)	96	1,564
Functional (DF=6)	144	2,346
Upper Limit of Quantification (ULOQ)		
Analytical	25,000	400,000
Functional (DF = 4)	100,000	1,600,000
Functional (DF=6)	150,000	2,400,000

Supplementary Table S2: Assay validation results for rat and cynomolgus monkey biological matrices based on criteria listed in Supplementary Table S3

	Rat			Cynomolgus Monkey		
	Plasma	**Serum**	**CSF**	**Plasma**	**Serum**	**CSF**
Validation Type	Full ('fit-for-purpose')	Bridging	Bridging	Bridging	Bridging	Bridging
Dilution Factor	4	4	6	6	6	6
INTRA-assay Precision & Accuracy	Passed	NF-L Passed UCH-L1 Failed	Passed	NF-L Passed UCH-L1 Failed	NF-L Passed UCH-L1 Failed	Passed
INTER-assay Precision & Accuracy	Passed	Not evaluated	Not evaluated	Not evaluated	Not evaluated	Not evaluated
Freeze/Thaw Stability	Passed 4 cycles at -80ºC	Not evaluated	Not evaluated	Not evaluated	Not evaluated	Not evaluated
Dilution Linearity	Passed	Passed	Passed	Passed	Passed	Passed

Supplementary Table S3: 'Fit-for-purpose' validation criteria

Test	Replicates	Samples	Criteria
INTRA-assay Precision & Accuracy	1 plate ≥ 3 replicates	**QC samples in matrix** • High [ ] • Mid [ ] • Low [ ] **Detection limits in diluent** • ULOQ • LLOQ	**For QCs:** CV ≤ 25% between replicates Bias = ± 25% **For ULOQ & LLOQ:** CV ≤ 25% between replicates Bias = ± 30%
INTER-assay Precision & Accuracy	3 plates ≥ 3 replicates	**QC samples in matrix** • High [ ] • Mid [ ] • Low [ ] **Detection limits in diluent** • ULOQ • LLOQ	**For QCs:** CV ≤ 25% between plates Bias = ± 25% **For ULOQ & LLOQ:** CV ≤ 25% between plates Bias = ± 30%
Freeze/Thaw Stability	1 plate 3 replicates	1-4 freeze/thaw cycles of High, Mid, and Low QC samples	Recovery vs. Initial Thaw = 75-125%
Dilution Linearity	1 plate 3 replicates	Serial dilution (2- to 64-fold) in matrix	$R^2 \geq 0.9$